Organic Geochemistry 135 (2019) 16–31

Contents lists available at ScienceDirect

Organic Geochemistry

journal homepage: www.elsevier.com/locate/orggeochem

Depth-related differences in archaeal populations impact the isoprenoid tetraether lipid composition of the Mediterranean Sea water column

Marc A. Besseling [a,*], Ellen C. Hopmans [a], Michel Koenen [a], Marcel T.J. van der Meer [a], Sanne Vreugdenhil [a], Stefan Schouten [a,b], Jaap S. Sinninghe Damsté [a,b], Laura Villanueva [a]

[a] NIOZ Royal Netherlands Institute for Sea Research, Department of Marine Microbiology and Biogeochemistry, and Utrecht University. P.O. Box 59, NL-1790 AB Den Burg, the Netherlands
[b] Utrecht University, Faculty of Geosciences, Department of Earth Sciences, P.O. Box 80.021, 3508 TA Utrecht, the Netherlands

ARTICLE INFO

Article history:
Received 13 February 2019
Received in revised form 6 June 2019
Accepted 22 June 2019
Available online 25 June 2019

Keywords:
Archaea
Thaumarchaeota
Marine Euryarchaeota group II
Isoprenoid GDGTs
TEX_{86}
Paleothermometer
Mediterranean Sea

ABSTRACT

Thaumarchaeota are one of the most abundant groups of Archaea in the marine water column. Their membrane consists of isoprenoid glycerol dibiphytanyl glycerol tetraethers (GDGTs) which are applied in the widely used TEX_{86} proxy to reconstruct past sea surface temperatures (SSTs). However, in some specific marine systems, such as the Mediterranean Sea, core-top TEX_{86}-derived temperatures do not seem to reflect annual mean SSTs. This has been attributed to contributions of deep-water dwelling Thaumarchaeota. Here, we investigate the potential causes of this bias by studying both the archaeal diversity as well as the intact polar lipid (IPL) GDGT composition in the Mediterranean water column by a combined 16S rRNA gene amplicon sequencing and a lipidomic approach on suspended particulate matter (SPM) at different water depths. The archaeal distribution showed a dominance of archaea other than Thaumarchaeota, i.e. Marine Euryarchaeota group II and III in the upper epipelagic waters (0–100 m deep), while Thaumarchaeota (Marine group I; MGI) dominated the subsurface and the deeper waters. This shift in the archaeal community composition coincided with a decrease in IPL GDGT-0 and increase of IPL crenarchaeol. The ratio of GDGT-2/GDGT-3 increased with water depth, but values were lower than observed in deep marine waters of some other regions. The increase of the GDGT-2/GDGT-3 ratio coincided with the high relative abundance of deep-water MGI, which may be linked to the high temperature and salinity found in specific water masses of the Mediterranean Sea. We conclude that these particularities of the Mediterranean Sea are responsible for the overestimated SST based on TEX_{86}.

1. Introduction

Archaea of the phylum Thaumarchaeota (also known as Marine group I, MGI) are among the most widespread and abundant prokaryotes in the marine realm (Karner et al., 2001; Francis et al., 2005; Teira et al., 2006). Their membrane lipids comprise archaeal glycerol dibiphytanyl glycerol tetraethers (GDGTs) with 0–4 cyclopentane moieties as well as the specific GDGT, crenarchaeol, with 4 cyclopentane moieties and a cyclohexane moiety, which is considered a specific biomarker for Thaumarchaeota (Sinninghe Damsté et al., 2002a, 2002b; for a review see Schouten et al., 2013). Members of the MGI are also capable of producing archaeol and methoxy-archaeol (Schouten et al., 2008; Elling et al., 2017). Importantly, the distribution of thaumarchaeotal GDGTs in the marine environment has been shown to be affected by temperature, i.e. with increasing temperature there is an increase in the relative abundance of cyclopentane-containing GDGTs and a specific isomer of crenarchaeol (cren′; Sinninghe Damsté et al., 2018). This has led to the development of the paleotemperature proxy TEX_{86} (TetraEther indeX of tetraethers consisting of 86 carbon atoms) for reconstruction of past sea surface temperatures (SSTs; Schouten et al., 2002). More recent and extended sediment core-top studies resulted in additional indices and novel calibrations (Kim et al., 2008, 2010; Tierney and Tingley, 2015).

Although there are many indications that the TEX_{86} signal of settling particles reaching the seafloor reflects the temperature of the upper epipelagic waters of the oceans, there are two main uncertainties. Firstly, the TEX_{86} signal may also be affected by

* Corresponding author.
E-mail address: marc.besseling@nioz.nl (M.A. Besseling).

https://doi.org/10.1016/j.orggeochem.2019.06.008
0146-6380/

input of archaea other than Thaumarchaeota, which could potentially synthesize some of the GDGTs involved in the TEX_{86} calculations. An earlier study has suggested that Marine group II Euryarchaeota (MGII) are significant contributors of GDGTs in oceanic surface waters based on the combination of core lipid (CL)-GDGT and 16S rRNA gene amplicon sequencing analyses (Lincoln et al., 2014). However, these findings have been challenged (Schouten et al., 2014) and there are no cultured representatives of the MGII group to confirm this hypothesis. Secondly, it has been suggested that TEX_{86} reflects subsurface temperature instead of SST because most MGI archaea reside in subsurface waters (50–200 m) (e.g., Huguet et al., 2007; Lopes dos Santos et al., 2010; Kim et al., 2012). Considering this, several studies have noted changes in the relative abundances of certain GDGTs (e.g., an increase of the relative abundances of GDGT with 2 vs 3 cyclopentane moieties) in marine suspended particulate matter (SPM) and surface sediments with increasing water depth (Taylor et al., 2013; Hernández-Sánchez et al., 2014; Kim et al., 2015). Although the increase of the GDGT-2/GDGT-3 ratio alone with depth does not affect TEX_{86} temperature, it does suggest the presence of a (thaum)archaeotal population in deeper waters with a different GDGT membrane composition than archaea existing in the subsurface waters and this may ultimately influence the sedimentary TEX_{86} signal.

In the Mediterranean Sea, this effect is particularly strong: the GDGT distribution in surface sediments strongly varies with water depth, even at relatively small spatial scales such as in the Balearic Sea (Kim et al., 2015). When the four GDGTs used in the TEX_{86} proxy were considered, the relative abundances of both GDGT-2 (and hence the GDGT-2/GDGT-3 ratio) and the crenarchaeol isomer increased with increasing water depth. These increases result in a bias towards higher TEX_{86} reconstructed temperatures compared to annual SSTs in deep-water surface sediments. The fact that this trend was also apparent in SPM collected at different water depths suggested that this change might be due to a change in the relative abundance of Thaumarchaeota species having different GDGT distributions in deep waters and that this signal is, at least partly, incorporated into sedimentary GDGTs. Kim et al. (2016) investigated the GDGT distribution in tandem with the diversity of Thaumarchaeota in the SPM of the Mediterranean outflow water sampled at the Portuguese margin at water depths of 100–1000 m. Similar to observations in the Mediterranean Sea itself, the relative abundances of both GDGT-2 and the crenarchaeol isomer increased with increasing water depth both in the core lipids (CLs) as well as in the intact polar lipids (IPLs; based on IPL-derived CL-GDGT analyses). Analysis of the genes encoding for the thaumarchaeotal ammonia monooxygenase (*amo*A) and an enzyme involved in the GDGT biosynthetic pathway revealed that there was an increasing contribution of 'deep water-dwelling' Thaumarchaeota with increasing water depth that could potentially explain the increase in relative abundance of both GDGT-2 and the crenarchaeol isomer. The combination of IPL-derived CL-GDGT analysis with a DNA-based approach targeting Thaumarchaeota in Kim et al. (2016) proved to be extremely useful for discerning the contribution of different thaumarchaeotal populations, but a potential contribution of other archaeal sources was not addressed.

Here, we study the archaeal community in the Mediterranean Sea water column by using 16S rRNA gene amplicon sequencing of DNA extracted from the SPM obtained from three stations (western, middle and eastern). We combined the analysis of the archaeal community composition with GDGT analyses by high resolution accurate mass/mass spectrometry [UHPLC–HRMS] with the aim to determine the archaeal sources of the isoprenoid GDGT pool present and their potential role explaining the bias of the TEX_{86} in the Mediterranean Sea.

2. Materials and methods

2.1. Sampling and physicochemical analyses

SPM was collected in the Mediterranean during the NESSC cruises in January and February 2016 on board of the R/V *Pelagia*. SPM was sampled at three stations (western station; 36°44′59.9″N 1°29′59.4″W, middle station; 34°58′09.0″N 18°06′47.1″E and the eastern station; 33°18′08″N 33°23′43″E, respectively; further referred to as stations 1, 2 and 3; Fig. 1). Samples were obtained from different water depths corresponding to different water masses in the Mediterranean Sea (Fig. 1). The upper water mass, the Modified Atlantic Water (MAW) is formed as a result of mixing Atlantic water with surface waters of the Alboran Sea (Gascard and Richez, 1985). Below the MAW the more saline intermediate water mass, the Levantine Intermediate Water (LIW), is present, which is formed in the Levantine Sea (Wüst, 1961). The LIW spreads out across the Mediterranean Sea and is the major contributor of the Mediterranean outflow into the Atlantic. The Mediterranean Sea is also known to contain open-ocean deep convections (e.g., Houpert et al., 2016). These convective processes result in deep water mass formation in the Mediterranean Sea (e.g., Castellari et al., 2000). The Western Mediterranean Deep Water (WMDW) formed in the Gulf of Lions (MEDOC group, 1970) and the Eastern Mediterranean Deep Water (EMDW) formed of Adriatic Deep Water (Pollak, 1951; Artegiani et al., 1997) and the Aegean Deep Water (Roether et al., 1996).

Three McLane WTS-LV in situ pumps (McLane Laboratories Inc., Falmouth, MA, USA) were deployed at various depths (Supplementary Table S1). Water (68–1545 L) was filtered using pre-ashed glass fiber (GF75) filters (Whatman, 0.3 μm pore size and 142 mm in diameter; Supplementary Table S1). Larger pore size (0.7 μm; GF/F) filters were also used at station 1 at 25, 40 and 100 m below sea level (mbsl; Supplementary Table S1). The filters were immediately stored at −80 °C after retrieval of the pumps.

A Sea-Bird SBE911+ conductivity–temperature–depth (CTD) system equipped with a 24 × 12 L Niskin bottle rosette sampler was used to collect continuous profiles of temperature, salinity and dissolved oxygen (O_2), the latter using a Sea-Bird oxygen electrode (Sea-Bird, WA, USA). A Chelsea Aquatracka MKIII fluorometer was used to record fluorescence (Supplementary Table S1). Dissolved inorganic nutrients were analyzed in water from Niskin bottles sub-sampled with 60 mL high-density polyethylene syringes with a three-way valve and filtered over Acrodisc PF syringe filters (0.8/0.2 μm Supor Membrane, PALL Corporation) into pre-rinsed 5 mL polyethylene vials. Water samples for the determination of the dissolved phosphate (PO_4^{3-}) and inorganic nitrogen (NO_3^-, NO_2^- and NH_4^+) concentrations were stored frozen at −20 °C until analyses upon return at NIOZ. Samples for dissolved reactive silicate (Si) analysis (Strickland and Parsons, 1968) were stored in the dark at 4 °C until analyses at NIOZ. The detection limits were PO_4^{3-} 0.007 μmol L^{-1}, NH_4^+ 0.03 μmol L^{-1}, NO_3^- + NO_2^- 0.01 μmol L^{-1} and NO_2^- 0.002 μmol L^{-1}.

2.2. Lipid extraction and analyses

Total lipids were extracted from SPM collected on 0.3 and 0.7 μm pore size glass fiber filters (samples taken at 25, 40 and 100 mbsl at station 1 were collected on 0.7 μm pore size glass fiber filters, the rest of the samples on 0.3 μm pore size glass fiber filters). After freeze-drying the filters were extracted using a modified Bligh and Dyer method as previously described by Schouten et al. (2008). C16-PAF (1-*O*-hexadecyl-2-acetoyl-*sn*-glycero-3-phosphocholine) was added as an internal standard after which the extracts were dried under a stream of nitrogen. The extracts

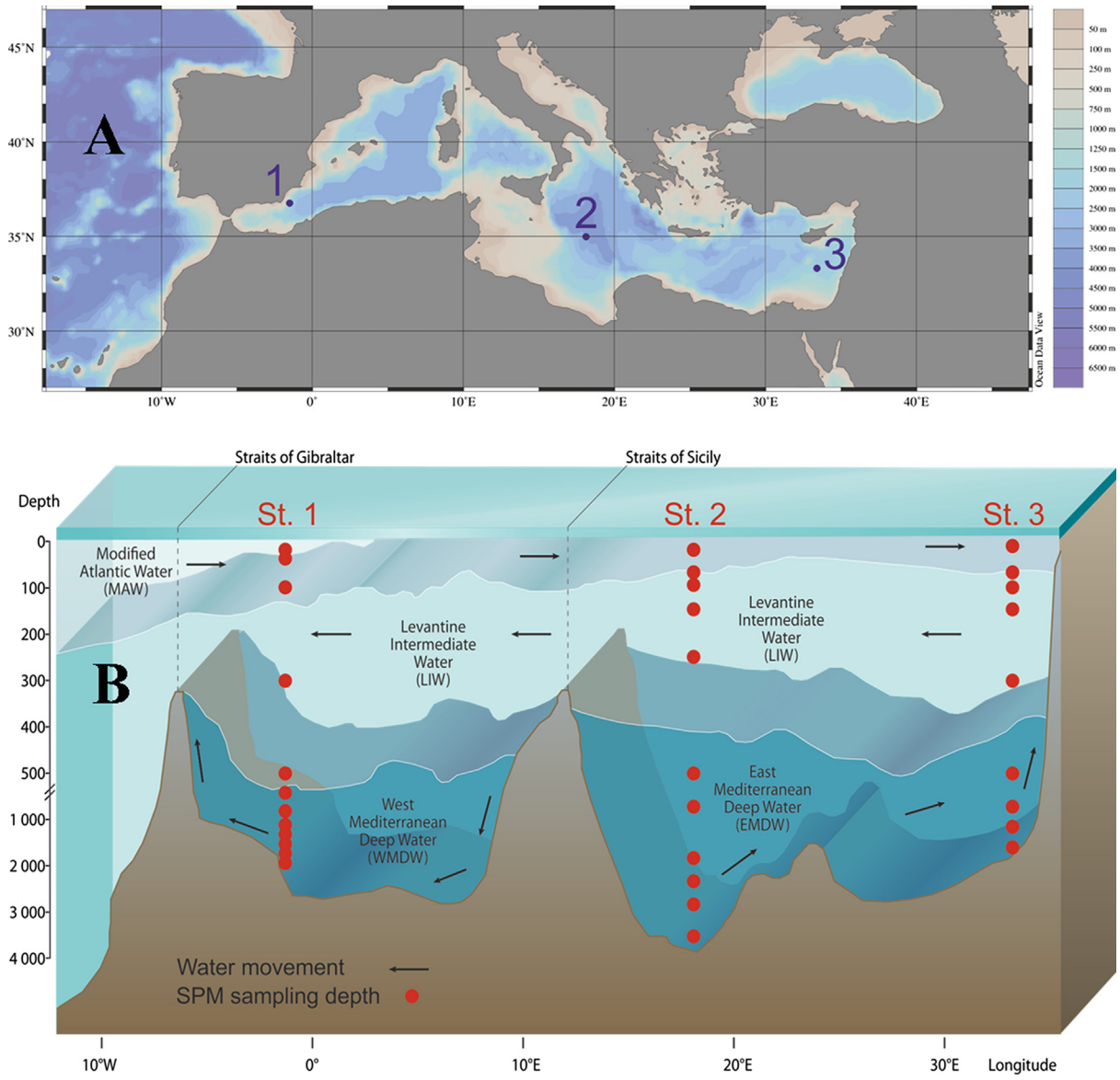

Fig. 1. (A) Map of the Mediterranean Sea revealing the locations of the sampling stations. Water depth is color indicated by the bathymetry legend on the right. (B) vertical distribution of Mediterranean Sea water masses. Modified from GRID-Arendal (http://www.grida.no/resources/5885) based on Hopkins (1985) and Zavaterelli and Mellor (1995). Note: depth axis is not to scale and note the break in the axis scale.

with the added standard were then dissolved by adding solvent (hexane:isopropanol:H_2O 718:271:10, v/v/v) and filtered through a 0.45 μm, 4 mm diameter True Regenerated Cellulose syringe filter (Grace Davison, Columbia, MD, USA).

IPLs were analyzed according to Besseling et al. (2018), a method based on Sturt et al. (2004). Briefly, samples were analyzed using an Ultimate 3000 RS UHPLC, equipped with thermostated auto-injector and column oven, couple to a Q Exactive Orbitrap MS with Ion Max source and heated electrospray ionization (HESI) probe (Thermo Fisher Scientific, Waltham, MA), was used. Separation was achieved on a YMC-Triart Diol-HILIC column (150 × 2.0 mm, 1.9 μm particles, pore size 12 nm; YMC Co., Ltd, Kyoto, Japan) with a guard column of the same material (10 × 2.1 mm). The same inclusion list was used as in Besseling et al. (2018). All samples were run in duplicate and the average IPL-GDGT distribution is reported, assuming identical response factors for all IPLs.

Peak areas for each individual IPL were determined by integrating the combined mass chromatogram (within 3 ppm) of the monoisotopic and first isotope peak of all relevant adducts formed (protonated, ammoniated and/or sodiated adducts may be formed in different proportions depending on the type of IPL). PAF was used to assess LC–MS performance and potential matrix effects. Absolute quantification of IPL GDGTs was not possible due to a lack of standards. IPLs of crenarchaeol and crenarcheol isomer are not separated and thus peak areas reported for any crenarchaeol IPL represents the sum of both isomers.

Bligh and Dyer extracts were dried under a stream of nitrogen and dissolved in a mixture of hexane:propanol (99:1, v/v) and filtered through 0.45 mm polytetrafluorethylene (PFTE) filters. GDGTs present in these extracts were analyzed on an Agilent 1260 UHPLC coupled to a 6130 quadrupole MSD in selected ion monitoring (SIM) mode, according to Hopmans et al. (2016). The injection volume was 10 μl and selected ion monitoring of the $[M+H]^+$ was used to detect the different GDGTs. C_{46} GDGT was used as an internal standard to quantify GDGTs (Huguet et al., 2006b).

For sea surface temperature (SST) reconstructions the TEX_{86}^H index was used as proposed by Kim et al. (2010). The TEX_{86}^H index

is a logarithmic function of the TEX_{86} index developed by Schouten et al. (2002):

$$TEX_{86}^{H} = \log \frac{[GDGT-2]+[GDGT-3]+[cren']}{[GDGT-1]+[GDGT-2]+[GDGT-3]+[cren']} \quad (1)$$

TEX_{86}^{H} values were converted to SSTs applying the deep restricted basin core top calibration (composed of Mediterranean Sea (Kim et al., 2015) and the northern Red Sea (Trommer et al., 2009) surface sediments collected at > 1000 mbsl) as suggested by Kim et al. (2015):

$$SST = 56.3 \times TEX_{86}^{H} + 30.2 \quad (2)$$

2.3. Nucleic acids extraction and quantitative PCR (QPCR) analyses

DNA was extracted from the glass fiber filters with the RNA PowerSoil® Total Isolation Kit plus the DNA elution accessory (Mo Bio Laboratories, Carlsbad, CA). the concentration of DNA was quantified by Nanodrop (Thermo Scientific, Waltham, MA). Archaeal 16S rRNA gene copies were estimated by quantitative PCR (QPCR) using the following primers: Parch519F and ARC915R (archaeal 16S rRNA gene), as previously described (Pitcher et al., 2011a, 2011b). For details on the QPCR conditions, efficiency and R^2 of the QPCR assays see Supplementary Table S2.

2.4. 16S rRNA gene amplicon sequencing, analysis, and phylogeny

PCR reactions were performed with the general prokaryotic primers S-D-Arch-0159-a-S-15 and S-D-Bact-785-a-A-21 (Klindworth et al., 2013) using 454 GLX sequencing with a single-ended approach as described in Moore et al. (2015). The archaeal 16S rRNA gene amplicon sequences were analyzed by QIIME v1.9 (Caporaso et al., 2010). Raw sequences were demultiplexed and then quality filtered with a minimum quality score of 25, length in the range 250–350, and allowing up to two mismatches in the barcode sequence. Taxonomy was assigned based on blast and the SILVA database version 128 (Altschul et al., 1990; Quast et al., 2013). Representative operational taxonomic units (OTUs; based on 97% sequence identity) sequences of archaeal groups were extracted through filter_taxa_from_otu_table.py and filter_fasta.py with QIIME (Caporaso et al., 2010). OTUs comprised of <50 16S rRNA gene amplicon reads were discarded. The phylogenetic affiliation of the partial archaeal 16S rRNA gene sequences was compared to release 128 of the Silva NR SSU Ref database (http://www.arb-silva.de/; Quast et al., 2013) using the ARB software package (Ludwig et al., 2004). Sequences were added to the reference tree supplied by the Silva database using the ARB Parsimony tool. Affiliation of any 16S rRNA gene sequences to a given subgroup was done assuming a similarity cutoff of ≥85%.

The water column was not evenly sampled in our study (with a higher density of sampling points in the (sub)surface in comparison to the deeper part of the water column; Fig. 1). In order to give a more realistic estimation of abundances of the archaeal OTUs in the Mediterranean water column, the archaeal copy number (16S rRNA gene copies L^{-1}) at a certain water depth was multiplied by the relative abundance of that specific OTU (in % of all archaeal reads). To minimize the bias of sampling resolution, the meters of the water column covering the distance between sampling points were multiplied by the abundance. The estimated abundances were then divided by the water column depths to get depth-integrated estimated abundances per OTU. These depth-integrated estimated abundances were used to rank the OTUs within each archaeal group, i.e. MGI, MGII and marine euryarchaeota group III (MGIII) and named accordingly (i.e. OTU-1 represents the most abundant within an archaeal group, OTU-2 s most, etc.). The three MG compositions, based on the depth-integrated abundances, at the three different stations were compared by Spearman's rank correlation coefficient analyses.

2.5. Clone library, sequencing and phylogenetic analyses of ammonia monooxygenase (amoA) coding gene fragments

The *amo*A gene fragments were amplified as described by Yakimov et al. (2011). The PCR mixture was the following (final concentration): Q-solution 1 × (PCR additive, Qiagen, Valencia, CA, USA); PCR buffer 1×; BSA (200 μg ml^{-1}); dNTPs (20 μM); primers (0.2 pmol μl^{-1}); $MgCl_2$ (1.5 mM); 1.25 U Taq polymerase (Qiagen). The PCR conditions for these amplifications were the following: 95 °C, 5 min; 35 × (95 °C, 1 min; 55 °C, 1 min; 72 °C, 1 min); final extension 72 °C, 5 min. The PCR products were gel-purified (QIAquick gel purification kit, Qiagen) and cloned in the TOPO-TA cloning® kit from Invitrogen (Carlsbad, CA, USA) and transformed in *Escherichia coli* TOP10 cells following the manufacturer's recommendations. Recombinant clones plasmid DNAs were purified by Qiagen Miniprep kit and screening by sequencing (n = 288) using M13R primer by BaseClear (Leiden, The Netherlands). Obtained archaeal *amo*A protein sequences were quality checked and aligned with already annotated *amo*A sequences by using the ClustalW Multiple alignment (Thompson et al., 1994): this resulted in n = 244 good quality sequences. A phylogenetic tree was constructed with MEGA7 (Kumar et al., 2016) with the neighbor-joining method (Saitou and Nei, 1987) with a bootstrap test of 1000 replicates. Phylogenetic trees were drawn using iTOL (Letunic and Bork, 2016).

2.6. Data availability

The CL- and IPL-GDGT data have been submitted to Pangaea. Sequence data of the partial 16S rRNA gene sequences have been submitted to the BioSample database under bioproject PRJNA524865 with accession no: SAMN12106735–SAMN12106766. Sequence data of partial *amo*A gene sequences have been submitted to the GenBank database under accession no: MK592163–MK592407.

3. Results

3.1. Physicochemistry of the water column

At stations 1, 2 and 3 (western, middle and eastern Mediterranean Sea; respectively; Fig. 1) water column SPM samples were taken at >10 different water depths, ranging between 25 and 3530 mbsl, during the winter of 2016. The water depth at these stations varied greatly (1963, 3609 and 1720 mbsl, respectively) due to the topography of the basin. The water column was fully oxygenated at all stations (oxygen levels of 172–252 μmol kg^{-1}) at the time of sampling. Salinity ranged between 37.9 practical salinity units (psu) and 39.1 psu (Supplementary Table S1). Ammonia concentrations declined with increasing depth at stations 1 and 3 (from 0.13 μmol L^{-1} at the surface to 0.10 μmol L^{-1} at the greatest depth and from 0.20 to 0.15 μmol L^{-1}, respectively), while in station 2 the levels increased from 0.10 to 0.18 μmol L^{-1} (Supplementary Table S1). Temperatures in the water column were in the range 13.1–14.1 °C at station 1, 13.9–17.2 °C at station 2 and 13.8–19.0 °C at station 3 (Supplementary Table S1). Concentration maxima of nitrite (NO_2^-) were detected at 40, 90 and 100 mbsl at stations 1, 2 and 3, respectively (Supplementary Table S1).

3.2. Archaeal abundance and diversity

Archaeal 16S rRNA gene abundance was estimated by quantitative PCR using general archaeal primers. At the surface (25 mbsl) of station 1, the copy number was 1.1×10^8 gene copies L^{-1} and increased sharply to 6.3×10^8 gene copies L^{-1} at 100 mbsl (Fig. 2). Maximum abundance was reached at 500 mbsl (8.3×10^8 gene copies L^{-1}), with a subsequent decline with increasing depth to 3.5×10^7 gene copies L^{-1} at 1300 mbsl (Fig. 2). At 1500 mbsl, another maximum was detected with 1.9×10^8 gene copies L^{-1}, and subsequently a decrease to 4.6×10^7 gene copies L^{-1} at 1900 mbsl (Fig. 2). At the surface (25 mbsl) of station 2, archaeal 16S rRNA gene abundance values were 5.4×10^7 gene copies L^{-1} and reached a maximum at 150 mbsl (3.4×10^8 gene copies L^{-1}). With increasing depth, values decreased to 1.7×10^7 gene copies L^{-1} at 1800 mbsl (Fig. 2). The abundance declined further to 7.7×10^5 gene copies L^{-1} at 3530 mbsl (Fig. 2). At station 3, the abundance at the surface (25 mbsl) was 4.6×10^7 gene copies L^{-1}, which was slightly higher than at 75 and 100 mbsl (Fig. 2). Maximum abundance was detected at 300 mbsl with 4.3×10^8 gene copies L^{-1}. It then declined to 2.3×10^5 gene copies L^{-1} at 1300 mbsl and sharply increased to 6.6×10^7 gene copies L^{-1} at 1700 mbsl (Fig. 2).

Based on the results of the 16S rRNA gene amplicon sequencing approach, the archaeal 16S rRNA gene reads were predominantly closely related to three archaeal lineages, the MGI Thaumarchaeota and MGII and III Euryarchaeota (Fig. 2). Minor groups, representing <4% of all archaeal reads, i.e. the Woesearchaeota from the superphylum DPANN (Rinke et al., 2013; Castelle et al., 2015) and marine benthic group A (MBG-A), were also detected. MGI was the major archaeal group for most of the water column (100 mbsl and deeper waters) representing 39–74% of all archaea (Fig. 2; Supplementary Table S6). In contrast, in surface waters, which contain an order of magnitude lower concentrations of archaeal cells, they represented only 15–33% of all archaea of the three stations. The surface waters (25–40 mbsl) at stations 1 and 2 were dominated by MGII (47–84%; Fig. 2 and Supplementary Table S6), while in surface waters (25 mbsl) of station 3 MGIII was the most abundant archaeal group (40%; Fig. 2). With increasing water depth, the relative abundance of MGII decreased to 24% (1900 mbsl), 15% (3530 mbsl) and 10% (1700 msbl) at stations 1, 2 and 3, respectively (Fig. 2). MGIII was less dominant at the subsurface (100–500 mbsl) compared to the surface of stations 2 and 3 with 3–25% relative abundance, MGIII was more dominant at the subsurface of station 1 (up to 7%) compared to the surface (Fig. 2). Relative abundances of MGIII increased at all three stations with increasing depth to 27%, 41% and 35% at stations 1, 2 and 3, respectively (Fig. 2).

Based on the 16S rRNA gene amplicon sequencing approach, 30 operational taxonomic units (OTUs; based on ≥97% sequence identity and with a >50 gene read cut-off) belonging to MGI were detected; these OTUs were present at all three stations (Supplementary Table S3). The five most abundant MGI OTUs in our dataset (estimated by multiplying the relative abundance (%) of reads for an OTU with archaeal 16S RNA abundance; see Materials and methods for details) together accounted for 67% of the estimated depth-integrated abundance of the 30 MGI OTUs detected. These OTUs differed in their niches in the water column as revealed in the heatmap of Fig. 3. Heatmaps for all 30 OTUs are shown in Supplementary Fig. S2 for each station. OTU-1, the overall most abundant OTU in our dataset (Supplementary Fig. S2), dominated in the bottom waters (for stations 1, 2 and 3 at 1900, 1800 and 1700 mbsl, respectively; Fig. 3 and Supplementary Fig. S2), while OTU-5 was predominant at the subsurface depths 25, 90 and 75 mbsl (Fig. 3 and Supplementary Fig. S2). Correlation between estimated abundances for the 30 OTUs at each station, based on Spearman's rho rank correlation coefficients (r_s), showed strong

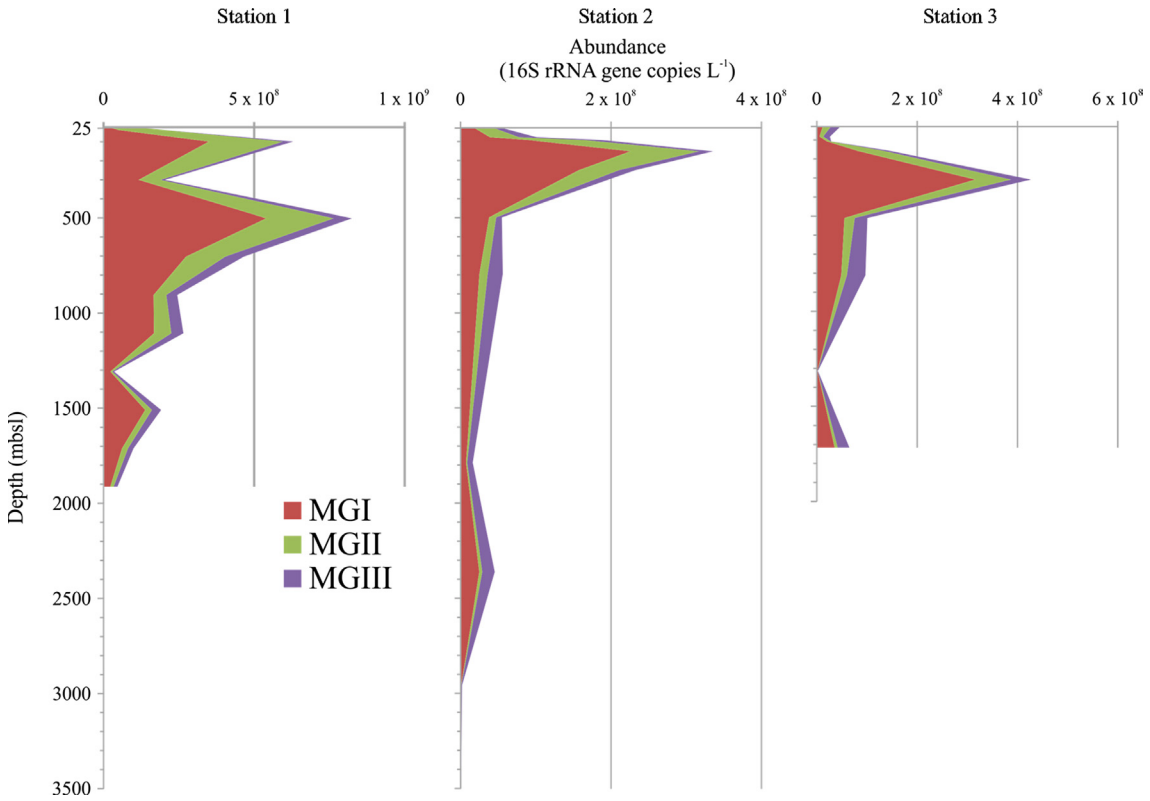

Fig. 2. Archaeal abundance profiles showing the absolute abundance (in archaeal 16S rRNA genes copies L^{-1} as determined by Q-PCR) for the three stations. Archaeal community composition for the three major groups of archaea is also given and based on 16S rRNA gene amplicon sequencing.

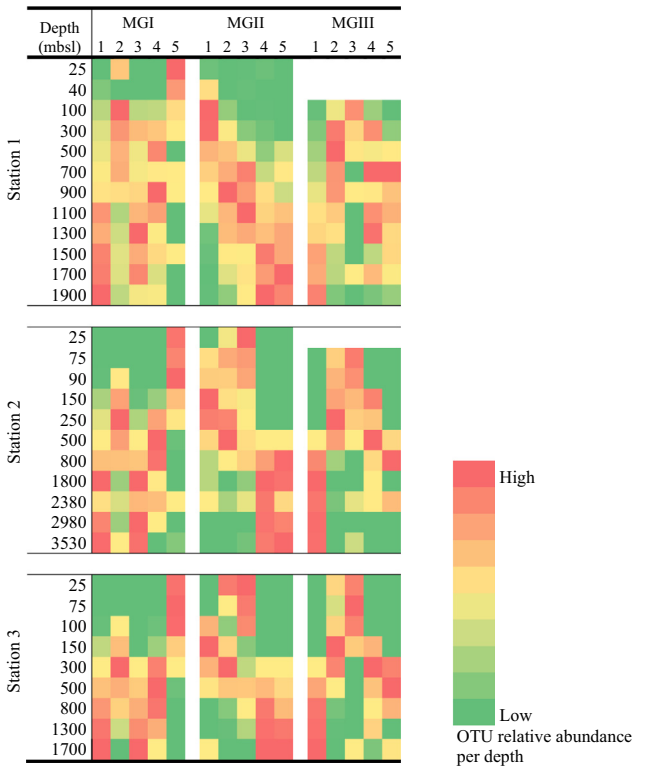

Fig. 3. Heatmap of the five most abundant operational taxonomic units (OTUs; based on ≥97% 16S rRNA gene similarity) of the three main archaeal groups (MGI–III) per station. Heatmap colors are indicative of the relative abundance per OTU per marine archaeal group (green = low relative abundance, red = high). MGIII OTUs (1–5) at station 1 (25 and 40 mbsl) and at station 2 (25 mbsl) are not shown because of low read numbers (<20 sequence reads). (For interpretation of the references to color in this figure legend, the reader is referred to the web version of this article.)

correlations between the MGI community composition of station 1 and of station 2 ($r_s = 0.80$, $\rho < 0.001$) and station 3 ($r_s = 0.74$, $\rho < 0.001$; Supplementary Table S3). MGI community composition between stations 2 and 3 were also highly correlated ($r_s = 0.89$, $\rho < 0.001$; Supplementary Table S3).

The phylogeny of the sequences of the MGI OTUs (Fig. 4) revealed that only a minor proportion (3 out of 30) of the OTUs were related to most cultivated MGI Thaumarchaeota (e.g., *Nitrosopumilus maritimus*) falling in cluster I, while the majority of OTUs were related to uncultured MGI species falling in clusters II and III (Fig. 4). The uncultured MGI OTUs are quite diverse and in many cases closely related to other marine uncultured MGI 16S rRNA gene sequences, often retrieved from greater water depths. The diversity of MGI OTUs was further investigated by sequencing the thaumarchaeotal *amo*A gene, encoding the alpha-subunit of the enzyme ammonia monooxygenase. We amplified and sequenced a fragment of the *amo*A gene by PCR at three different depths at each station (one in epipelagic, one in mesopelagic and one in bathypelagic waters; for station 1: at 100, 500 and 1500 mbsl, for station 2: at 150, 800 and 2380 mbsl, for station 3: at 25, 300 and 1700 mbsl). Phylogeny and classification was based on a recent *amo*A gene database (La Cono et al., 2018). Throughout the water column, diverse MGI communities were detected and classified as 'shallow' and 'deep' water type based on their *amo*A gene sequence (Fig. 5) and amino acid differences (e.g., Supplementary Fig. S8) (cf. Francis et al., 2005; Hallam et al., 2006; Mincer et al., 2007; Beman et al., 2008). We detected a clear shift from dominance of the 'shallow water' *amo*A type to predominance of the 'deep water' *amo*A type with increasing depth at all three stations (Fig. 5). The 'shallow water' group of *amo*A gene sequences contained 2 subclusters and the 'deep water' group contained 4 subclusters (Supplementary Fig. S7A and B; cf. La Cono et al., 2018; Sintes et al., 2016). A minor proportion of *amo*A gene sequences predominantly present in the upper surface water (25 mbsl, obtained at station 3) grouped into subcluster 1 (Supplementary Fig. S7A), comprising *amo*A gene sequences of surface dwelling *Nitrosopumilus* (i.e. *Candidatus* N. adriaticus and *Ca.* N. piranensis; Bayer et al., 2016), as well as *amo*A gene sequences of *Ca.* Nitrosopumilus koreensis and *Ca.* N. sediminis isolated from marine sediments (Park et al., 2014). Most of the 'surface-dwelling' MGI Thaumarchaeota detected in the epipelagic zone were grouped into subcluster 2 (Supplementary Fig. S7A). This subcluster contains *amo*A sequences from all three stations and from all depths (except from 1700 mbsl at station 3; Fig. 5). Most of the obtained *amo*A gene sequences were clustered in the 'deep water' group, with the majority grouped into subcluster 3, lower relative abundances were clustered in subgroup 4, 5 and 6 (Supplementary Fig. S7B). As the 'deep water' group only contains uncultured Thaumarchaeota, their *amo*A sequences cannot be linked to cultured Thaumarchaeota as observed for the MGI 16S rRNA gene sequences.

Thirteen MGII OTUs (again defined on the basis of ≥97% sequence identity) were identified at the three stations (Fig. 3 and Supplementary Fig. S3). OTU-1 of MGII (the most dominant MGII OTU overall) was most abundant within the bathypelagic zone (>1000 mbsl) for all three stations (Fig. 3). OTU-2 was most dominant at the subsurface (100–300 mbsl) for all three stations (Fig. 3). OTU-3 was dominant (based on the relative abundance) in surface waters of stations 2 and 3 but was mostly detected at greater depths (500–1300 mbsl) at station 1 (Fig. 3). MGII communities between the three stations were compared by correlating the estimated abundances of the 19 OTUs per station. The MGII community composition was only weakly correlated between station 1 and stations 2 and 3 ($r_s = 0.60$, $\rho < 0.05$ and $r_s = 0.49$, $\rho < 0.1$, respectively; Supplementary Table S3). However, between station 2 and 3, the MGII community composition showed a stronger correlation ($r_s = 0.87$, $\rho < 0.001$; Supplementary Table S3).

Six MGIII OTUs were detected in the water column of the three stations (Fig. 3 and Supplementary Fig. S4). OTU-1 of MGIII was detected mostly within the bathypelagic zone (>1000 mbsl) at all three stations (Fig. 3). The highest relative abundance of MGIII OTU-2 was detected at the subsurface (250 and 150 mbsl for stations 2 and 3, respectively) or within the mesopelagic zone (500 mbsl at station 1; Fig. 3). OTU-3 was most dominant in surface waters (0–100 mbsl) at all three stations (Fig. 3). A significant correlation, based on Spearman's rho rank correlation coefficients, of the estimated abundances of the six MGIII OTUs was observed between the three stations ($r_s = 0.89$, $\rho < 0.05$; Supplementary Table S8).

3.3. Archaeal lipid abundance and distribution in the water column

The archaeal intact polar lipids (IPLs) consisted of GDGT-0 to GDGT-4 and crenarchaeol with monohexose (MH), dihexose (DH) and hexose-phosphohexose (HPH) headgroups (Fig. 6). Other archaeal membrane IPLs (including archaeol IPLs) were targeted in the UHPLC–HRMS analysis but not detected (for a list of targeted IPLs, see Besseling et al., 2018). The IPL-GDGTs were detected in all SPM samples with the exception of the surface waters of station 2 (25 and 75 mbsl) and at 75 mbsl of station 3 (Fig. 6). Maximum concentrations of IPL-GDGTs (expressed in response units L^{-1}) were detected in subsurface waters (i.e. at stations 1 and 3 at 300 mbsl and at station 2 at 250 mbsl) (Fig. 6). For station 1, only HPH-GDGTs with GDGT-0 and crenarchaeol core lipid were detected (53% and 47% relative abundance, respectively; Fig. 6) at 25 mbsl. At 40 mbsl, the headgroup DH was also observed in combination with GDGT-1, GDGT-2 and crenarchaeol (Fig. 6). At 100 mbsl, the majority of IPL-GDGTs detected had the headgroup DH

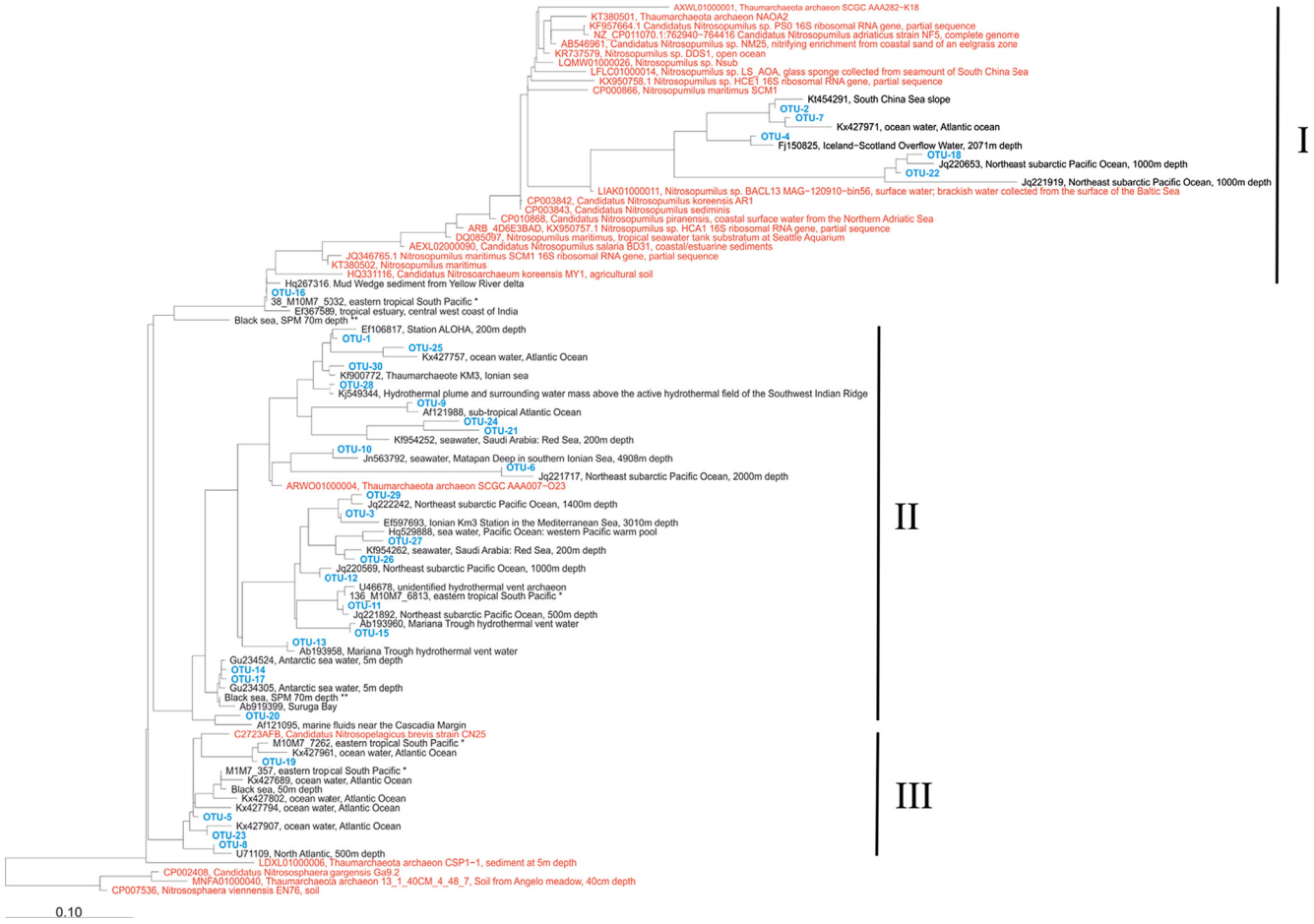

Fig. 4. Phylogenetic tree composed of 16S rRNA gene amplicon sequences of marine group I (MGI) operational taxonomic units (OTUs; in blue) detected in suspended particulate matter (SPM) of the Mediterranean Sea. Closely affiliated sequences from uncultured MGI members (in black) and from MGI cultures and from with metagenomics assembled MGI environmental genomes (both in red) are also included. Three distint subgroups are indicated which were used for the comparison with other archaeal subgroups and intact polar lipid (IPL-) glycerol dialkyl glycerol tetraether lipids (GDGTs) distributions, shown in Table 1. Scale bar represents a 10% sequence dissimilarity. (For interpretation of the references to color in this figure legend, the reader is referred to the web version of this article.)

but also IPL-GDGTs with the headgroup MH, in combination with CLs GDGT-0 and crenarchaeol (Fig. 6) were detected. For station 2, IPLs with GDGT-0, GDGT-2 and crenarchaeol were detected with the headgroups DH (DH-GDGT-2) or with HPH (HPH-GDGT-0 and HPH-crenarchaeol) at 90 mbsl (Fig. 6). At 150 mbsl, the majority of IPLs contained a DH headgroup and this remained the dominant headgroup with increasing depth (Fig. 6). At station 3, IPL-GDGTs were detected at 25 mbsl but not at 75 mbsl. The IPLs at 25 mbsl consisted mostly of the headgroup HPH in combination with GDGT-0 and crenarchaeol. A minor abundance of DH GDGT-2 was also observed. Generally, with increasing depth, the relative abundance of HPH-IPLs decreased and DH-IPLs increased (Fig. 6).

The summed concentration of core lipid (CL-) GDGTs (i.e. GDGTs present without a head group) was on average highest at station 1 (ranging from 70 to 820 pg L^{-1}) with a maximum at 100 mbsl (Fig. 7). Summed concentrations of CL GDGTs in stations 2 and 3 ranged from 20 to 160 pg L^{-1} and 30 to 190 pg L^{-1}, respectively, (Fig. 7) with maxima at 250 and 300 mbsl, respectively (Fig. 7). After the maximum in the concentration profile, all stations showed a steady decrease in CL GDGT concentrations with increasing depth (Fig. 7). CL archaeol was detected in concentrations <5% of the summed GDGTs. The distribution of the CL-GDGTs (Fig. 8) showed less variation over the water column than the GDGT core distribution of the IPLs (see above). Crenarchaeol was the most abundant GDGT with a relative abundance ranging from 50 to 59%, followed by GDGT-0, ranging from 14 to 32% (Fig. 8). Other detected GDGTs were GDGT-1 to GDGT-4 and cren′ (Fig. 8). GDGT-3 and GDGT-4 were generally only minor compounds, with the exception of GDGT-3 at 75 mbsl at station 3 (12%). The relative abundance of GDGT-2 increased with greater depth at stations 1 and 3, up to 300 mbsl. However, this increase was much less apparent at station 2 (Fig. 8). GDGT-1 relative abundances increased at stations 2 and 3, up to 250 and 300 mbsl, respectively (Fig. 8). Cren′ relative abundances increased up to 250 mbsl at station 2 and up to 300 mbsl at stations 1 and 3, but for station 1 this increase was less apparent (Fig. 8). The relative abundance of GDGT-0 decreased with greater increasing depth (up to 250 mbsl at station 2 and up to 300 mbsl at stations 1 and 3) and increased with greater depth below 500 mbsl at station 2; this increase was not observed at the other stations (Fig. 8).

Surface sediments (0–1 cm) underlying the sampled stations were also analyzed for their CL-GDGT distribution. Sedimentary CL GDGTs were dominated by crenarchaeol followed by GDGT-0 at all three stations. The distribution of CL GDGTs in the surface sediments highly correlates ($r \geq 0.99$) with the CL GDGTs composition of the overlying water column.

3.4. TEX_{86}^{H} temperature reconstructions

TEX_{86}^{H} values were calculated based on the CL GDGTs in the surface sediments collected below the studied water columns.

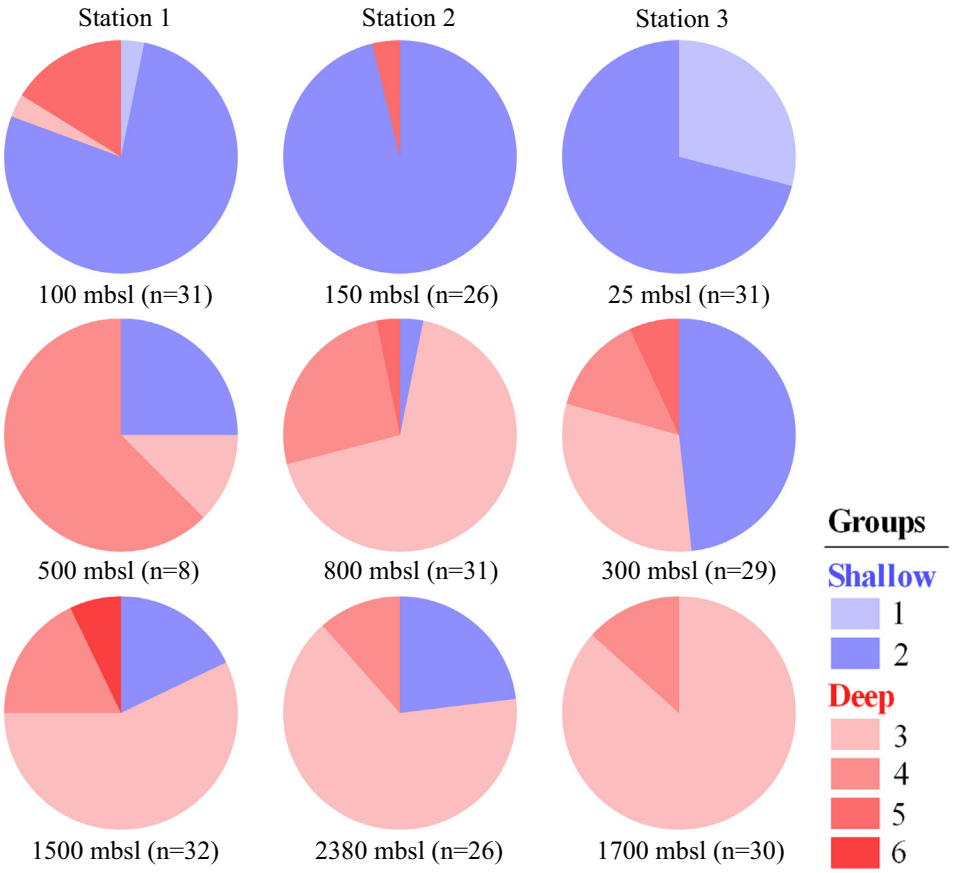

Fig. 5. Pie charts showing the fractional abundance of specific groups of sequences of the α-subunit of the ammonia monooxygenase (*amo*A) gene from clone libraries obtained at three different depths at all three stations. Groups are clustered as 'shallow' *amo*A gene (indicated in blue; groups 1and 2) and 'deep' *amo*A gene (indicated in red; groups 3–6) types. Colors resemble the groups as indicated in the phylogenetic trees (Supplementary Fig. S1A and S1B). Sampling depth is given underneath the pie charts with the number (n =) of sequences that were obtained in the clone libraries. (For interpretation of the references to color in this figure legend, the reader is referred to the web version of this article.)

At station 1, the TEX_{86}^{H} value was −0.187 ± 0.001 (standard deviation, obtained by analyzing three different surface sediment samples per station). This resulted in a TEX_{86}^{H} temperature of 19.7 °C (calculated using the specific Mediterranean calibration of Kim et al., 2015). At station 2, the TEX_{86}^{H} value was −0.131 ± 0.001, which corresponds to a TEX_{86}^{H} temperature of 22.8 °C. At station 3, the TEX_{86}^{H} value was −0.132 ± 0.002, with a TEX_{86}^{H} temperature of 22.8 °C.

4. Discussion

4.1. A diverse archaeal community composition throughout the water column

In this study, we observed distinctly different distributions of the archaeal groups MGI, II and III throughout the Mediterranean water column. In our study, the same dominant archaeal OTUs were detected with fairly similar distributions among the three stations (Fig. 3; Supplementary Figs. S2–S4), despite the vast horizontal distance between them, suggesting that the distribution of these OTUs at our three stations can be taken as representative of the archaeal diversity and distribution throughout the Mediterranean Sea. In agreement with our work, De Corte et al. (2009) showed that the archaeal community composition was highly stratified with depth in the eastern Mediterranean Sea and associated with different water masses. Galand et al. (2010) reported a strong seasonality of the archaeal community composition within shallow coastal NW Mediterranean Sea water, with a dominance of Euryarchaeota in winter. Our samples were also obtained in winter (January and February), and within surface waters (25 mbsl) either MGII (stations 1 and 2) or MGIII (station 3) Euryarchaeota were dominant (Fig. 2 and Supplementary Fig. S4), in agreement with the study of Galand et al. (2010). The dominance of Euryarchaeota within the surface waters of the Mediterranean Sea has also previously been observed (Tamburini et al., 2009; Zhou et al., 2018). This is compatible with their potential metabolism, as determined from metagenomics, which suggests that they might be able to use light-derived energy and cope well with UV radiation stress (Frigaard et al., 2006; Iverson et al., 2012; Martin-Cuadrado et al., 2014). From 100 m downwards, MGII and MGIII Euryarchaeota still contribute a substantial part of the total archaeal population with values ranging from 27 to 56% of the total archaea (Fig. 2). Certain OTUs of the MGII and MGIII Euryarchaeota show, however, a preference for deep waters (>1500 mbsl), i.e. OTU-1 (Fig. 3). Deep-water samples collected in this study (from 500 m downwards) correspond to the West Mediterranean Deep Water (WMDW, station 1), and the East Mediterranean Deep Water (EMDW, stations 2 and 3) water masses. These stations are all characterized by relatively high bottom water temperatures (e.g., 13–14 °C; Supplementary Table S1), which remain >12.5 °C year round (Wüst, 1961), which is considerably warmer than deep water temperatures in the global ocean (Sverdrup et al., 1942).

The higher irradiance and UV-induced stress in surface waters, which favors the Euryarchaeota, is believed to have a negative influence on the surface water abundance of MGI Thaumarchaeota,

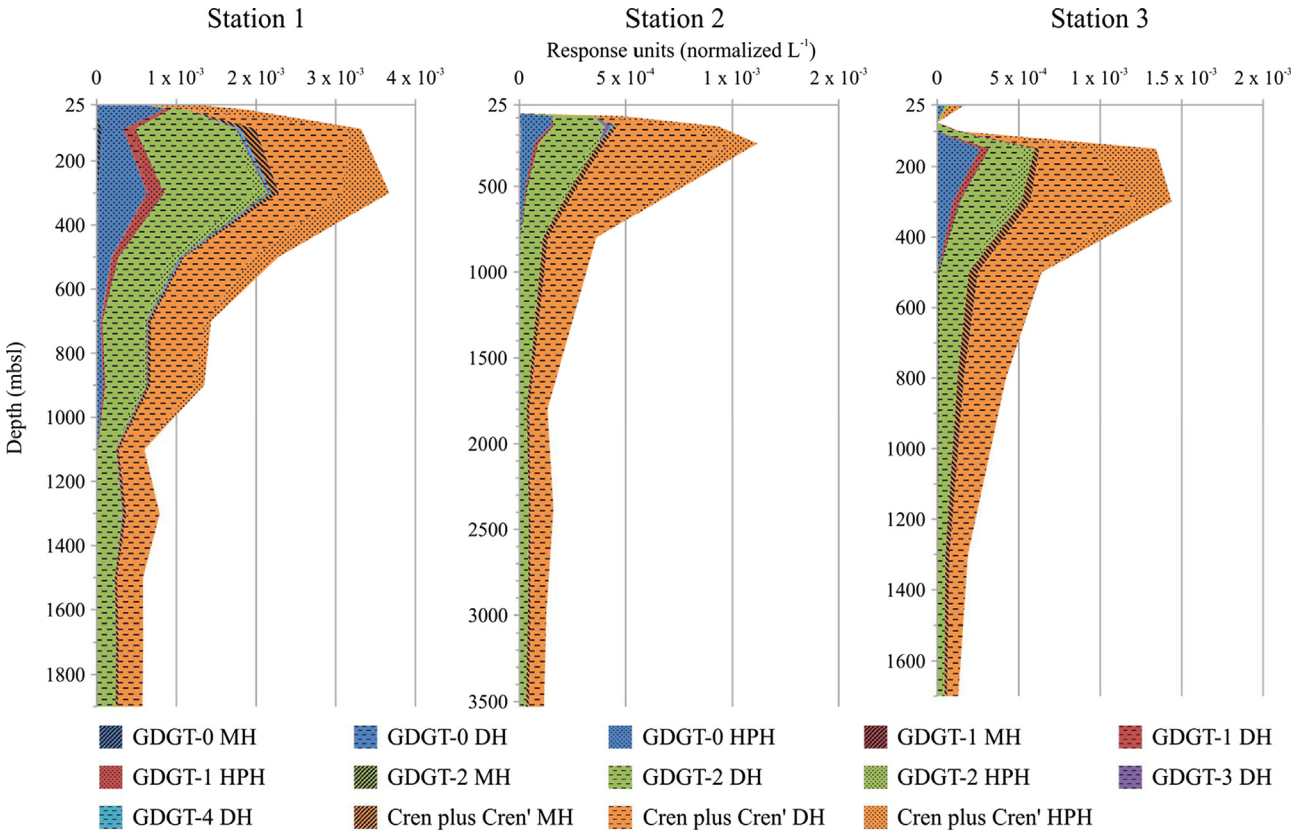

Fig. 6. Depth profiles of the concentration (indicated by the response units per L) of the most abundant intact polar lipid (IPL-) glycerol dialkyl glycerol tetraether lipids (GDGTs) for the three stations. The overall profile shows the sum of the IPLs.

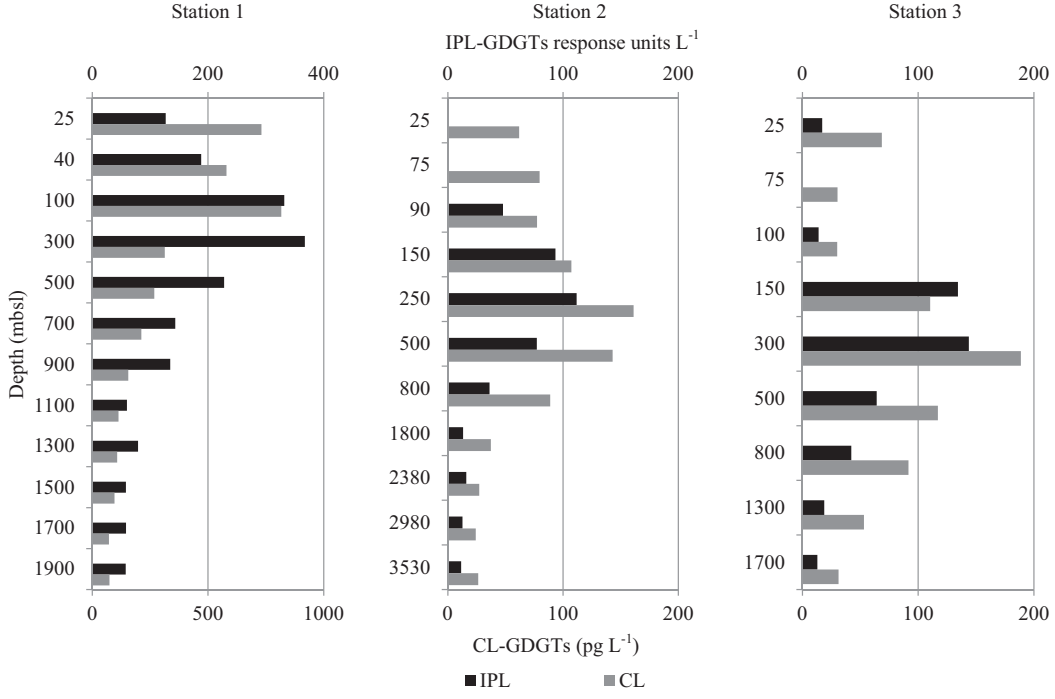

Fig. 7. Absolute abundance profiles of intact polar lipid (IPL-) and core lipid (CL-) glycerol dialkyl glycerol tetraether lipids (GDGTs) abundance in the water column of the three stations. The IPL-GDGT abundance (black bars) is indicated in response units per L (upper axis), CL-GDGT abundance (grey bars) is indicated in pg L^{-1} (lower axis).

which are known to have a niche preference for subsurface waters (approximately 50–500 m depth, (Massana et al., 2000; Pitcher et al., 2011b; Beman et al., 2012; Lincoln et al., 2014; Sollai et al., 2018). Indeed, our study shows that MGI archaea have a much higher abundance (both relative and absolute) in subsurface waters (100–300 mbsl) compared to the surface (0–100 mbsl),

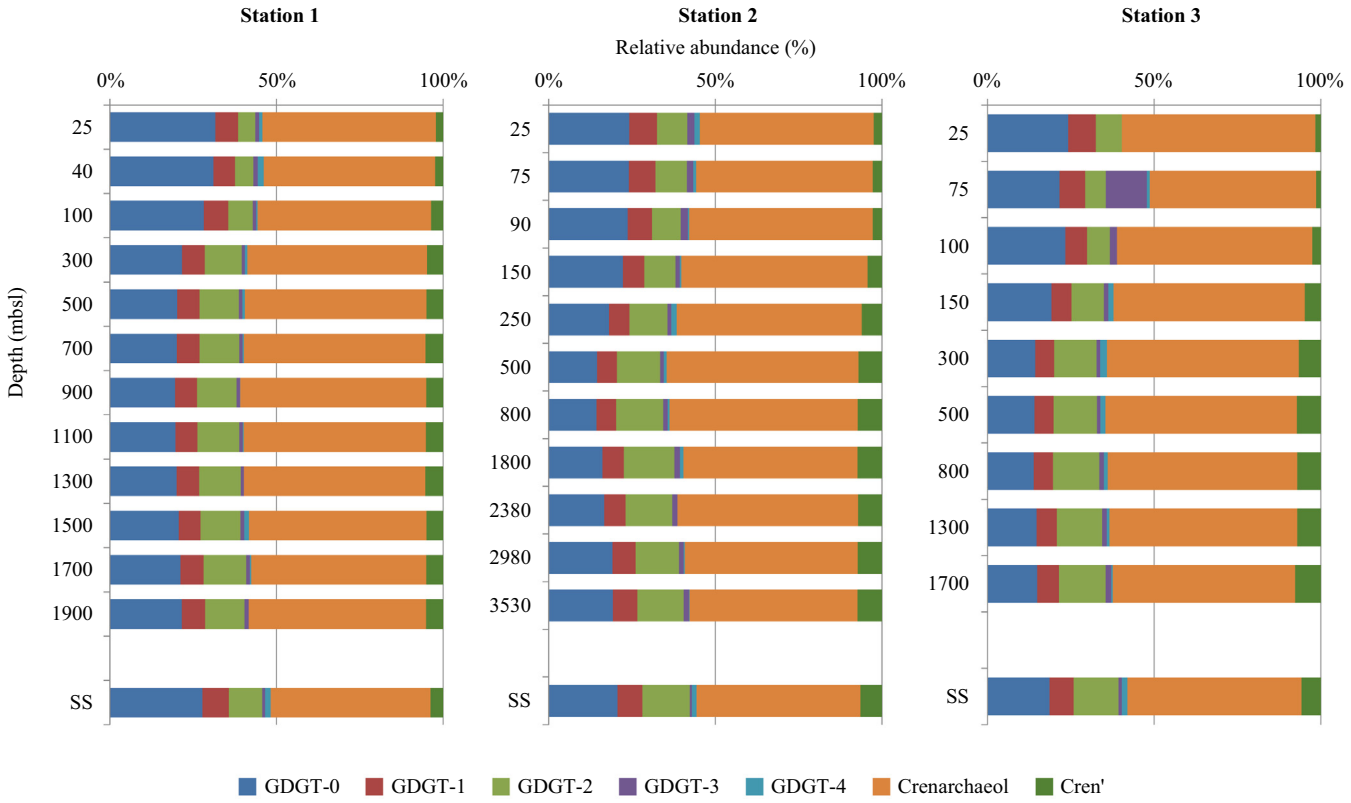

Fig. 8. Depth profiles of the relative abundance of seven detected core lipid (CL-) glycerol dialkyl glycerol tetraether lipids (GDGTs) for the three stations and the CL-GDGT composition of the underlying surface sediments (SS).

but are also found up to 500 m depth. This is different from the North Atlantic where the maximum abundance of Thaumarchaeota is typically located at around 100 m depth and then consistently decreased with increasing depth (Herndl et al., 2005). Thus, in the Mediterranean there exists an expanded, deeper niche for MGI Thaumarchaeota, which coincides with the Levantine Intermediate Waters (LIW) and the underlying deep water masses in the Mediterranean Sea water column (Fig. 2). Indeed, Techtmann et al. (2015) already reported MGI Thaumarchaeota as dominant members of the prokaryotic community within the LIW and the Eastern Mediterranean Deep Water (EMDW) and concluded that their high relative abundance was indicative of the LIW. The LIW which is flowing from the eastern to the western basin at approximately 100–600 m depth is characterized by a (relatively) high salinity and temperature (38.5–39.1 psu and 13.3–18.9 °C, respectively) in comparison with similar depths in other ocean basins. These could be the physicochemical factors favoring an increased abundance of MGI Thaumarchaeota in these deeper water masses.

Specific MG1 OTUs, i.e. OTU-5, were present from the surface to approximately 500 m depth, comprising both the surface Modified Atlantic Water (MAW) as well as the LIW (Fig. 3). The 16S rRNA gene sequences of these OTUs are closely related to thaumarchaeotal 16S rRNA gene sequences previously detected in the Black Sea surface (Sollai et al., 2018) and in the Atlantic Ocean (Bergauer et al., 2018) (Fig. 4). The close phylogenetic association of these thaumarchaeotal OTUs with thaumarchaeotal 16S rRNA gene sequences previously detected in marine waters with high salinity and temperature regimes suggests that these OTUs might be thaumarchaeotal species better adapted to these conditions. Specific thaumarchaeotal MGI OTUs were preferentially found in deep waters (e.g., OTU-1 and OTU-2; Fig. 3), indicating a clear niche difference for various thaumarchaeotal OTUs. Changes in the diversity of MGI Thaumarchaeota throughout the water columns are also evident from the observed variations in ammonia monooxygenase (*amo*A) gene sequences, which have been previously used to classify Thaumarchaeota as 'shallow' and 'deep water' type (e.g., Francis et al., 2005; Beman et al., 2008; Yakimov et al., 2011; Sintes et al., 2013). In the Mediterranean Sea, the shallow *amo*A cluster dominated at the surface (25 mbsl, station 3) and subsurface (100 and 150 mbsl, stations 1 and 2, respectively; Fig. 5), with sequences closely related to sequences previously detected in, for example, the Mediterranean (accession number MF662834 in Fig. 6; La Cono et al., 2018), Antarctic coastal waters (EU239020; Kalanetra et al., 2009) and Monterey Bay, California (DQ148839; Francis et al., 2005). In the deeper waters (>300 mbsl) *amo*A gene sequences falling in subclusters 3–6 dominated; these subclusters are affiliated to those of deep-water Thaumarchaeota (Sintes et al., 2016; La Cono et al., 2018; Supplementary Fig. S7). Little is known about the physiology of the deep-water MGI Thaumarchaeota since there are currently no cultured representatives. Their niche has been previously linked to much reduced ammonium concentrations in deep waters requiring distinct *amo*A genes (Sintes et al., 2016; Supplementary Fig. S8). An adaptation of the ammonia monooxygenase enzyme could increase the affinity towards ammonia or even broaden the spectrum of available substrates as proposed by Smith et al. (2016). However, the Mediterranean Sea is characterized by (ultra)oligotrophic conditions (Krom et al., 1991) and the ammonia concentrations are low throughout the water column (e.g., at station 1: 0.02–0.13 μmol L^{-1}; Supplementary Table S1). It could be that the high affinity for ammonia by Thaumarchaeota is causing these low ammonia concentrations. However, this conversion of ammonia likely would have resulted in an increase of nitrite concentrations in the water column which was not observed (Supplementary Table S1). Therefore it is hard to

imagine that the observed niche differentiation of Thaumarchaeota in the Mediterranean Sea is actually linked to differences in ammonia affinity attributed to the deep-water Thaumarchaeota.

Although the deep-water masses West Mediterranean Deep Water (WMDW) and East Mediterranean Deep Water (EMDW) originate from different locations, the deeper water MGI community compositions were similar (Fig. 3); i.e., in the three stations the dominant Thaumarchaeotal MGI OTU was OTU-1 (>50% average relative abundance in the deeper water masses; Supplementary Table S2). The physical properties of the WMDW and the EMDW were similar at the sampling locations and during the time of sampling (Supplementary Table S1), including NH_4^+ concentrations, suggesting the Thaumarchaeota MGI OTUs found in the deep water basins of the Mediterranean Sea are also adapted to this niche, independent of the original provenance of the water mass. Time of sampling in this case, even for the deep-water masses, was probably a determining factor for the archaeal community composition. Winter et al. (2009) also showed that the deep archaeal community was affected by vertical mixing in the Mediterranean Sea and that this seasonal effect could be as dynamic as observed at the surface.

4.2. Archaeal lipid composition in the water column of the Mediterranean Sea

In our study, we screened for a wide range of known and potential head group combined with archaeal core lipids (see Besseling et al. (2018) for a list of targeted compounds). However, only the IPLs with head groups MH, DH and HPH in combination with different CL-GDGTs were detected (Fig. 6). The concentration of these summed IPLs peaked at all three stations at 250–300 mbsl and were substantially lower in surface (0–100 m; except for Station 1) and deeper (>500 m) waters (Fig. 7), generally in good agreement with the depth distribution of the abundance of archaeal copy numbers (Fig. 2). No archaeal IPLs were detected at 25 and 75 mbsl at station 2 and at 75 mbsl at station 3, which is probably due to the analytical detection limits. A lower abundance of most IPL-GDGTs in surface (<80 mbsl) than in deeper waters has been previously observed in the Black Sea (Schubotz et al., 2009) and in the Western Atlantic Ocean (Hurley et al., 2018).

The IPL-GDGTs in the surface waters at 25–40 mbsl in station 1 and at 25 m at station 3 were mostly dominated by GDGT-0 and crenarchaeol carrying the HPH headgroup. HPH crenarchaeol has been hypothesized as a biomarker for living (Pitcher et al., 2011a, 2011b; Buckles et al., 2013) and active Thaumarchaeota (Elling et al., 2014). MGI DNA was detected at these depths, but in much lower amounts compared to the subsurface (Fig. 2). However, the dominance of HPH crenarchaeol suggest that these GDGTs are produced by present, albeit less abundant, MGI cells. With increasing depth (i.e. >40 mbsl, through the MAW, the LIW and the deepest water masses), the relative abundance of DH IPLs increased, especially for the IPLs with GDGT-2 and crenarchaeol and its isomer as CLs (Fig. 6). This may be due to a preferential synthesis of glycosidic IPL-GDGTs due to a physiological adaptation of the producers. Elling et al. (2014) showed differences in the IPL-GDGT composition in different growth phases of the thaumarchaeon *Nitrosopumilus maritimus* with HPH-GDGTs preferentially produced in the early growth phase compared to later growth phases. Furthermore, *N. maritimus* also shows different head group compositions with respect to pH, with relatively more HPH head groups compared to glycosidic head groups at a higher pH (Elling et al., 2015). However, *N. maritimus* and two other Thaumarchaeota isolates showed clear differences in head group compositions when grown under identical conditions, implying that species composition also affect the IPL compositition (Elling et al., 2015).

Interestingly, the relative abundances of IPLs with a GDGT-0 core decreased with increasing depth in all three stations (Fig. 8). This is contrary to other marine waters in which the archaeal IPL composition in SPM has been determined. For example, the relative abundance of IPL-GDGT-0 increased with water depth in the Arabian Sea (Schouten et al., 2012), and in parts of the Western Atlantic Ocean (Hurley et al., 2018). A possible explanation is the headgroup composition of GDGT-0 IPLs, which is predominantly the (presumably) more labile headgroup HPH instead of MH and DH (Fig. 6). These differences may be also be caused by differences of the archaeal community composition present at various water depths in the Mediterranean Sea.

4.3. Biological sources of archaeal lipids in the water column

To assess potential sources of specific IPLs, we correlated the abundance of archaea falling in specific subgroups (OTUs were grouped in subgroups based on phylogenetic similarity; Fig. 4, Supplementary Figs. S2 and S3) with the most abundant archaeal IPLs (Table 1) following the approach of Sollai et al. (2018). The absolute abundance of specific archaeal groups (estimated by multiplying the total archaeal 16S rRNA gene copies L^{-1} by the relative abundances of the archaeal groups and by assuming one 16S rRNA gene copy number per genome) was correlated with the absolute abundances of archaeal IPLs expressed as response units per liter (Table 1). Significant positive correlations (ρ-value < 0.05) for all three stations (Table 1) were found between MGI subgroup I and HPH-GDGTs and DH-GDGTs, driven mostly by DH-GDGT-2 and DH-crenarchaeol. On the other hand, MGI subgroup II is also correlated with DH-crenarchaeol (Table 1). MGI subgroup III was only significantly correlated with HPH-GDGT-0 at all three stations (Table 1; correlations with p-values < 0.05 are highlighted). The observed correlations suggest that these thaumarchaeotal groups are the biological source of most IPLs. However, culture studies have shown that Thaumarchaeota synthesize mainly IPLs with GDGT-0 and crenarchaeol as core lipids, as well as GDGT-1 to GDGT-4 in lower relative abundance (Sinninghe Damsté et al., 2002a, 2012; Schouten et al., 2008; Pitcher et al., 2011a; Elling et al., 2014). However, our data reveal that GDGT-2 and crenarchaeol, and perhaps its isomer (cren′), are the main core lipids in IPL-GDGTs, especially from 90 m downwards (Fig. 6), while IPL-GDGT-0 would be expected to be also high, as seen before in other marine waters, such as the Portuguese margin (Kim et al., 2016). This particularity seems to be restricted to the MGI populations in the Mediterranean Sea. It is possible that these Thaumarchaeota regulate their lipid membrane composition in a different way, or alternatively, their lipid membrane composition varies between the different phylogenetic groups within the MGI archaea present in the Mediterranean Sea. In this regard, the similarity between major OTUs of MGI found in the Mediterranean Sea water masses with those found in similar physicochemical conditions (i.e. high salinity and temperature as in the Red Sea) could explain the observed similarity in GDGT composition between the Mediterranean and the northern Red Sea (Kim et al., 2015) and the dissimilarity with open ocean systems and Thaumarchaeotal cultures studied so far.

The abundance of MGII and III archaea were also positively correlated with the concentrations of HPH and DH-GDGTs (Table 1), which may suggest that they also contribute to the GDGT pool. However, the absence of IPL-GDGTs in the surface waters dominated by MGII/MGIII suggest that these archaeal groups are not a major source for these lipids, in contrast to previous suggestions (Lincoln et al., 2014), and instead might synthesize membrane lipids not included in our analytical window. Indeed, it has been suggested that MGII/MGIII might synthesize mixed bacterial/archaeal-like membranes based on the presence of bacterial mem-

Table 1
Table with correlation values of the abundance of specific archaeal subgroups with those of most common archaeal intact polar lipid (IPL-) glycerol dialkyl glycerol tetraether lipids (GDGTs) for the three stations. The correlation data were obtained by applying Spearman ranking correlation coefficient analyses. The IPLs with a dihexose (DH) or a hexose-phosphohexose (HPH) head group were also summed and correlated against the MG subgroups. Correlation coefficient values with a ρ-value < 0.05 are highlighted.

	HPH	DH	HPH-GDGT-0	DH-GDGT-2	HPH-GDGT-2	DH-crenarchaeol	HPH-crenarchaeol
Station 1							
MGI Group I	**0.86**	**0.82**	0.42	**0.78**	0.57	**0.83**	0.49
MGI Group II	0.46	**0.79**	−0.05	**0.76**	**0.80**	**0.82**	0.05
MGI Group III	**0.94**	**0.60**	**0.71**	0.56	0.28	**0.60**	**0.75**
MGII Group I	**0.84**	**0.75**	0.50	**0.73**	**0.68**	**0.78**	0.56
MGII Group II	**0.67**	**0.96**	0.15	**0.97**	0.56	**0.95**	0.14
MGII Group III	−0.49	0.10	−**0.74**	0.07	0.10	0.12	−**0.65**
MGII Group IV	**0.58**	−0.01	**0.73**	0.00	−0.06	0.00	**0.70**
MGIII Group I	**0.60**	**0.88**	0.07	**0.87**	**0.74**	**0.90**	0.12
MGIII Group II	−0.35	0.22	−**0.66**	0.16	0.30	0.25	−0.54
Station 2							
MGI Group I	**0.88**	**0.88**	**0.70**	**0.84**	**0.75**	**0.72**	**0.75**
MGI Group II	**0.68**	**0.68**	0.07	0.55	0.43	**0.81**	0.14
MGI Group III	0.36	0.36	**0.77**	0.46	0.49	0.07	**0.78**
MGII Group I	**0.72**	**0.72**	**0.68**	**0.72**	**0.69**	0.55	**0.74**
MGII Group II	**0.75**	**0.75**	**0.79**	**0.75**	**0.77**	0.57	**0.83**
MGII Group III	0.53	0.53	0.14	0.43	−0.01	0.42	0.10
MGII Group IV	−0.45	−0.45	−0.23	−0.45	−0.19	−0.40	−0.23
MGIII Group I	**0.72**	**0.72**	0.56	**0.67**	**0.73**	0.60	**0.61**
MGIII Group II	0.39	0.39	−0.27	0.26	0.05	0.60	−0.21
Station 3							
MGI Group I	**0.98**	**0.98**	0.48	**0.90**	**0.84**	**0.98**	0.58
MGI Group II	**0.95**	**0.97**	0.33	**0.88**	**0.83**	**1.00**	0.50
MGI Group III	0.23	0.31	**0.71**	0.51	0.62	0.18	0.66
MGII Group I	**0.80**	**0.88**	0.61	**0.90**	**0.84**	**0.79**	**0.73**
MGII Group II	**0.90**	**0.90**	0.41	**0.83**	**0.84**	**0.93**	0.51
MGII Group III	0.44	0.37	−0.26	0.21	0.02	0.48	−0.28
MGII Group IV	0.05	−0.11	**0.71**	−0.07	0.12	−0.22	0.65
MGIII Group I	0.65	0.63	0.64	0.62	**0.82**	0.60	**0.82**
MGIII Group II	0.53	0.49	−0.32	0.24	0.05	0.58	−0.22

brane lipid biosynthetic genes compared to archaeal ones (Villanueva et al., 2017). As cultures of these archaea are still lacking, no definite conclusions can be made at this point regarding the possible contribution of the MGII/MGIII to the IPL-GDGT pool present in the marine water column. The positive correlation between MGII and III and the specific GDGTs mentioned above could be due to the fact they share their niche with MGI Thaumarchaeota as indicated in the correlation matrix of the archaeal groups (based on the summed relative abundances of the grouped OTUs; Supplementary Fig. S9).

4.4. Implications for the TEX_{86} paleothermometer

The TEX_{86} paleothermometer is based on the fractional abundances of the CLs GDGT-1–3, and the crenarchaeol isomer in sediments (Schouten et al., 2002). The assumption for the use of this proxy is that the CL-GDGTs in sediments are primarily derived from GDGTs produced in surface waters, presumably because the GDGTs produced in surface waters are more easily transported to the sediment than those produced in deeper waters through grazing and fecal pellet formation (Huguet et al., 2006a). Kim et al. (2015, 2016) showed that in the Mediterranean Sea and in waters of the Portuguese margin, strongly affected by the outflowing Mediterranean LIW and WMDW, the GDGT distribution in sediments was unusually affected by GDGTs produced in deeper waters. Our detailed study allows us to further evaluate this. The CL-GDGT distribution in SPM changes clearly with depth (Supplementary Fig. S12), with an increase in the relative abundance of GDGT-2 and the crenarchaeol isomer and a decrease of GDGT-1, in agreement with scattered SPM data reported by Kim et al. (2015). In the surface sediments the relative abundance of GDGT-2 and the crenarchaeol isomer is less than in SPM from deeper waters but still higher than in SPM from the surface waters. The opposite is true for GDGT-1, with a higher relative abundance in surface waters compared to that in the surface sediments. Although we don't know if this distribution is influenced by seasonal factors, the data suggest that surface CL-GDGTs are transported to the sediment but that CL-GDGTs from deeper waters also contribute to some extent. This is in good agreement with the IPL data, which show that IPL-GDGTs are primarily produced in subsurface waters (with a maximum at 250–300 mbsl) and that the main CLs are GDGT-2 and crenarchaeol. Transformation to CL-GDGTs from these IPLs by loss of the polar head groups could explain the observed changes with depth in the CL-GDGT profiles in the water column.

An increase in the GDGT-2/GDGT-3 ratio, based on the CL-GDGTs, with increasing water depth has been previously reported for multiple marine settings (e.g., Taylor et al., 2013; Hernández-Sánchez et al., 2014) including the Mediterranean Sea (Kim et al., 2015). Although changes in this ratio do not affect values of TEX_{86}, they have been interpreted as an indicator of GDGT production by Archaea living in the deeper part of the water column. In our data set, the GDGT-2/GDGT-3 ratio also increases with increasing depth (Fig. 9). However, GDGT-2/GDGT-3 values within the deeper part (300 mbsl and downwards; located in the LIW, the WMDW and the EMDW) of the Mediterranean Sea were generally lower than observed in SPM from other regions, such as the North Atlantic Ocean (Turich et al., 2007; Basse et al., 2014; Hurley et al., 2018), the South Atlantic Ocean (Hernández-Sánchez et al., 2014; Hurley et al., 2018), the Cariaco Basin (Zhu et al., 2016), the Black Sea (Zhu et al., 2016), the North Pacific (Zhu et al., 2016) and the equatorial Pacific (Zhu et al., 2016) (Fig. 9). Furthermore, it remained stable from 300 to 500 mbsl downwards, which is different from observations in the Atlantic Ocean, where the GDGT-2/GDGT-3 ratio increases with depth (Fig. 9). The relatively low GDGT-2/GDGT-3 values and the constant values with depth in

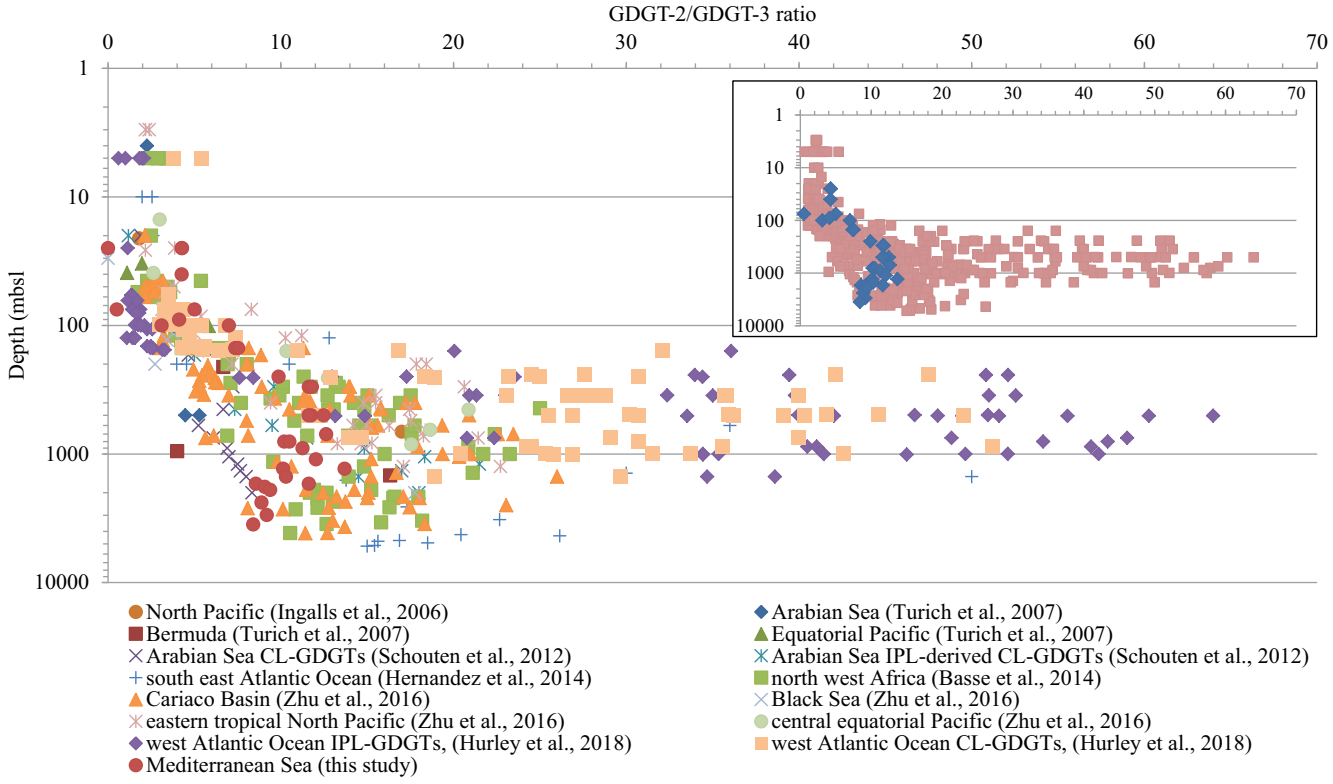

Fig. 9. Depth profile of the ratio between glycerol dialkyl glycerol tetraether lipids (GDGTs) with two and three cyclopentane moieties (GDGT-2/GDGT-3) from core lipid (CL-) GDGTs from all three stations (indicated by red circles). For reference, the GDGT-2/GDGT-3 ratios (from CL-GDGTs, intact polar lipid (IPL-) GDGTs and IPL derived CL-GDGTs) for other water columns in multiple marine environments are also plotted. Note the logarithmic Y-axis. The inset distinguishes the data points from this study (blue diamonds) and the data points from the other studies (red squares). (For interpretation of the references to color in this figure legend, the reader is referred to the web version of this article.)

the Mediterranean Sea could be due to the relatively high and constant in situ temperatures throughout the water column compared to the global open ocean.

As noted before for the Mediterranean Sea, the deviating CL-GDGT distribution in sediments due to a larger contribution of deep water dwelling Thaumarchaeota has consequences for the TEX_{86} paleotemperature proxy (Kim et al., 2015). Accordingly, Kim et al. (2015) developed a specific Mediterranean Sea core top calibration using only deep water sediments. We applied this calibration to the underlying surface sediments, but the reconstructed temperatures were only slightly higher (1.1 °C at both stations) than the recorded annual mean SSTs at station 1 and 3, respectively (Supplementary Fig. S5), which is just outside the calibration error of 1 °C (Kim et al., 2015). Only at the station with the deepest water column there is a larger offset (4 °C; Supplementary Fig. S5). This station (3609 m deep) was the deepest station and perhaps the expanded deep water column attributed to the larger offset of the reconstructed SST. In fact sediments at >3000 m water depth were not included in the deep water calibration by Kim et al. (2015). Furthermore, the estimated total abundance of archaea at depths > 1000 mbsl is approximately one order of magnitude lower than the maximum abundance detected in the subsurface waters (100–500 m depth), which suggests that the potential contribution to the archaeal lipid pool of deep water archaea may still be significant. This potential contribution of archaeal lipids, formed in the deeper parts of the Mediterranean Sea and the Portuguese Margin, to the sedimentary record has previously been proposed by Kim et al. (2015, 2016).

Surprisingly, Menzel et al. (2006) reported for Mediterranean Pliocene sapropels lower than expected TEX_{86}-based SST values using the common Schouten et al. (2002) calibration and suggested that this could be caused by the oxycline rising up into the photic zone, which substantially affects the composition of the Thaumarchaeotal community. A recent study by Polik et al. (2018) has confirmed these results with additional analyses of Mediterranean Pliocene and Pleistocene sapropels. The characteristic GDGT distributions within these sapropels and the modern Mediterranean were interpreted to be caused by different Thaumarchaeota community compositions (Polik et al., 2018). Our study highlights the complexity and internal variability within the modern thaumarchaeotal community that is not limited to the "shallow" and "deep" water types previously described. Furthermore, when a shallow oxycline develops during times of sapropel formation, the Thaumarchaeotal composition and distribution may be much more like that of the present day Black Sea (cf. Sollai et al., 2018) than the present-day oxic Mediterranean with major consequences for the type of calibration that should be used for TEX_{86} paleothermometry. The niche occupancy and thriving of these MGI subgroups in different water masses in the Mediterranean Sea may explain the deviations in SST-derived from TEX_{86} observed both in the past and in the present, and also shows the importance of understanding the thaumarchaeotal community dynamics in situ to get a better understanding on the effects of environmental factors on the GDGT distribution and therefore on the TEX_{86} paleothermometer.

5. Conclusions

We studied the IPL and CL-GDGT distribution in combination with the archaeal community composition of the Mediterranean Sea water column at three different stations, one in the western basin and two in the eastern basin. We detected a dominance of MGII and MGIII archaea at the surface of the water column,

whereas MGI dominated the subsurface and the deeper parts of the water column. We detected specific thaumarchaeotal OTUs, which could be adapted to the relative high temperature and salinity found in the LIW mass of the Mediterranean Sea. These thaumarchaeotal OTUs, which seem to proliferate in the specific conditions in the LIW water mass of the Mediterranean Sea, are most likely causing the different archaeal lipid signals that translate to higher TEX_{86} values than observed in the open ocean with similar SSTs. No evidence was found that archaeal groups such as MGII and MGIII archaea, shown to be present by genetic evidence, contribute substantially to the GDGT signal, and they are therefore not expected to affect TEX_{86} calculations. The CL-GDGT distribution was characterized by an increase of the GDGT-2/GDGT-3 ratio with depth as observed in other marine systems, but with relatively low GDGT-2/GDGT-3 values compared to other oceans may possibly be due to the particularities of the Mediterranean Sea (i.e. high salinity and temperature of specific water masses). Future studies focused on the enrichment/culture of the specific deep water MGI OTUs found in this study, followed by lipid analysis, should clarify their role in the deep water archaeal GDGT distribution in the Mediterranean Sea.

Acknowledgments

We acknowledge the cruise leader, captain, crew, and participants of NESSC cruises 64PE406 and 64PE407 for sampling and technical support. Elda Panoto is acknowledged for technical support and NIOZ for the PhD grant for MAB to LV. This research was further supported by the NESSC and SIAM Gravitation Grants (024.002.001 and 024.002.002) from the Dutch Ministry of Education, Culture and Science (OCW), the European Research Council (ERC) under the European Union's Horizon 2020 research and innovation program (grant agreement no. 694569 – MICROLIPIDS) to JSSD and the Netherlands Organisation for Scientific Research (NWO) (Middelgroot grant no. 834.13.004) to ECH. We thank the reviewers for their helpful comments.

Appendix A. Supplementary material

Supplementary data to this article can be found online at https://doi.org/10.1016/j.orggeochem.2019.06.008.

Associate editor—**Andrew Revill**

References

Altschul, S.F., Gish, W., Miller, W., Myers, E.W., Lipman, D.J., 1990. Basic local alignment search tool. Journal of Molecular Biology 215, 403–410.
Artegiani, A., Paschini, E., Russo, A., Bregant, D., Raicich, F., Pinardi, N., Artegiani, A., Paschini, E., Russo, A., Bregant, D., Raicich, F., Pinardi, N., 1997. The Adriatic Sea general circulation. Part II: Baroclinic circulation structure. Journal of Physical Oceanography 27, 1515–1532.
Basse, A., Zhu, C., Versteegh, G.J.M., Fischer, G., Hinrichs, K.-U., Mollenhauer, G., 2014. Distribution of intact and core tetraether lipids in water column profiles of suspended particulate matter off Cape Blanc, NW Africa. Organic Geochemistry 72, 1–13.
Bayer, B., Vojvoda, J., Offre, P., Alves, R.J.E., Elisabeth, N.H., Garcia, J.A.L., Volland, J.M., Srivastava, A., Schleper, C., Herndl, G.J., 2016. Physiological and genomic characterization of two novel marine thaumarchaeal strains indicates niche differentiation. The ISME Journal 10, 1051–1063.
Beman, J.M., Popp, B.N., Alford, S.E., 2012. Quantification of ammonia oxidation rates and ammonia-oxidizing archaea and bacteria at high resolution in the Gulf of California and eastern tropical North Pacific Ocean. Limnology and Oceanography 57, 711–726.
Beman, J.M., Popp, B.N., Francis, C.A., 2008. Molecular and biogeochemical evidence for ammonia oxidation by marine Crenarchaeota in the Gulf of California. The ISME Journal 2, 429–441.
Bergauer, K., Fernandez-Guerra, A., Garcia, J.A.L., Sprenger, R.R., Stepanauskas, R., Pachiadaki, M.G., Jensen, O.N., Herndl, G.J., 2018. Organic matter processing by microbial communities throughout the Atlantic water column as revealed by metaproteomics. Proceedings of the National Academy of Sciences of the United States of America 115, E400–E408.
Besseling, M.A., Hopmans, E.C., Boschman, R.C., Sinninghe Damsté, J.S., Villanueva, L., 2018. Benthic archaea as potential sources of tetraether membrane lipids in sediments across an oxygen minimum zone. Biogeosciences 15, 4047–4064.
Buckles, L.K., Villanueva, L., Weijers, J.W.H., Verschuren, D., Sinninghe Damsté, J.S., 2013. Linking isoprenoidal GDGT membrane lipid distributions with gene abundances of ammonia-oxidizing Thaumarchaeota and uncultured crenarchaeotal groups in the water column of a tropical lake (Lake Challa, East Africa). Environmental Microbiology 2, 1–18.
Caporaso, J.G., Kuczynski, J., Stombaugh, J., Bittinger, K., Bushman, F.D., Costello, E.K., Fierer, N., Peña, A.G., Goodrich, J.K., Gordon, J.I., Huttley, G.A., Kelley, S.T., Knights, D., Koenig, J.E., Ley, R.E., Lozupone, C.A., McDonald, D., Muegge, B.D., Pirrung, M., Reeder, J., Sevinsky, J.R., Turnbaugh, P.J., Walters, W.A., Widmann, J., Yatsunenko, T., Zaneveld, J., Knight, R., 2010. QIIME allows analysis of high-throughput community sequencing data. Nature Methods 7, 335–336.
Castellari, S., Pinardi, N., Leanman, K., 2000. Simulation of water mass formation processes in the Mediterranean Sea: Influence of the time frequency of the atmospheric forcing. Journal of Geophysical Research 105, 24157–24181.
Castelle, C.J., Wrighton, K.C., Thomas, B.C., Hug, L.A., Brown, C.T., Wilkins, M.J., Frischkorn, K.R., Tringe, S.G., Singh, A., Markillie, L.M., Taylor, R.C., Williams, K.H., Banfield, J.F., 2015. Genomic expansion of domain Archaea highlights roles for organisms from new phyla in anaerobic carbon cycling. Current Biology 25, 1–12.
De Corte, D., Yokokawa, T., Varela, M.M., Agogué, H., Herndl, G.J., 2009. Spatial distribution of *Bacteria* and *Archaea* and *amo*A gene copy numbers throughout the water column of the Eastern Mediterranean Sea. The ISME Journal 3, 147–158.
Elling, F.J., Konneke, M., Lipp, J.S., Becker, K.W., Gagen, E.J., Hinrichs, K.U., 2014. Effects of growth phase on the membrane lipid composition of the thaumarchaeon *Nitrosopumilus maritimus* and their implications for archaeal lipid distributions in the marine environment. Geochimica et Cosmochimica Acta 141, 579–597.
Elling, F.J., Könneke, M., Mußmann, M., Greve, A., Hinrichs, K.-U., 2015. Influence of temperature, pH, and salinity on membrane lipid composition and TEX_{86} of marine planktonic thaumarchaeal isolates. Geochimica et Cosmochimica Acta 171, 238–255.
Elling, F.J., Könneke, M., Nicol, G.W., Stieglmeier, M., Bayer, B., Spieck, E., de la Torre, J.R., Becker, K.W., Thomm, M., Prosser, J.I., Herndl, G.J., Schleper, C., Hinrichs, K.U., 2017. Chemotaxonomic characterisation of the thaumarchaeal lipidome. Environmental Microbiology 19, 2681–2700.
Francis, C.A., Roberts, K.J., Beman, J.M., Santoro, A.E., Oakley, B.B., 2005. Ubiquity and diversity of ammonia-oxidizing archaea in water columns and sediments of the ocean. Proceedings of the National Academy of Sciences of the United States of America 102, 14683–14688.
Frigaard, N.U., Martinez, A., Mincer, T.J., DeLong, E.F., 2006. Proteorhodopsin lateral gene transfer between marine planktonic Bacteria and Archaea. Nature 439, 847–850.
Galand, P.E., Gutiérrez-Provecho, C., Massana, R., Gasol, J.M., Casamayor, E.O., 2010. Inter-annual recurrence of archaeal assemblages in the coastal NW Mediterranean Sea (Blanes Bay Microbial Observatory). Limnology and Oceanography 55, 2117–2125.
Gascard, J.C., Richez, C., 1985. Water masses and circulation in the Western Alboran Sea and in the Straits of Gibraltar. Progress in Oceanography 15, 157–216.
Hallam, S.J., Mincer, T.J., Schleper, C., Preston, C.M., Roberts, K., Richardson, P.M., DeLong, E.F., 2006. Pathways of carbon assimilation and ammonia oxidation suggested by environmental genomic analyses of marine Crenarchaeota. PLoS Biology 4, 520–536.
Hernández-Sánchez, M.T., Woodward, E.M.S., Taylor, K.W.R., Henderson, G.M., Pancost, R.D., 2014. Variations in GDGT distributions through the water column in the South East Atlantic Ocean. Geochimica et Cosmochimica Acta 132, 337–348.
Herndl, G.J., Reinthaler, T., Teira, E., Aken, H. Van, Veth, C., Pernthaler, A., Pernthaler, J., 2005. Contribution of Archaea to total prokaryotic production in the deep Atlantic Ocean. Applied and Environmental Microbiology 71, 2303–2309.
Hopkins, T.S., 1985. Physics of the sea. In: Margalef, R. (Ed.), Key Environments: West Mediterranean. Pergamon Press, New York, pp. 100–125.
Hopmans, E.C., Schouten, S., Sinninghe Damsté, J.S., 2016. The effect of improved chromatography on GDGT-based palaeoproxies. Organic Geochemistry 93, 1–6.
Houpert, L., Durrieu de Madron, X., Testor, P., Bosse, A., D'Ortenzio, F., Bouin, M.N., Dausse, D., Le Goff, H., Kunesch, S., Labaste, M., Coppola, L., Mortier, L., Raimbault, P., 2016. Observations of open-ocean deep convection in the northwestern Mediterranean Sea: Seasonal and interannual variability of mixing and deep water masses for the 2007–2013 period. Journal of Geophysical Research: Oceans 121, 8139–8171.
Huguet, C., Cartes, J.E., Sinninghe Damsté, J.S., Schouten, S., 2006a. Marine crenarchaeotal membrane lipids in decapods: Implications for the TEX_{86} paleothermometer. Geochemistry, Geophysics, Geosystems 7. https://doi.org/10.1029/2006GC001305.
Huguet, C., Hopmans, E.C., Febo-Ayala, W., Thompson, D.H., Sinninghe Damsté, J.S., Schouten, S., 2006b. An improved method to determine the absolute abundance of glycerol dibiphytanyl glycerol tetraether lipids. Organic Geochemistry 37, 1036–1041.
Huguet, C., Schimmelmann, A., Thunell, R., Lourens, L.J., Sinninghe Damsté, J.S., Schouten, S., 2007. A study of the TEX_{86} paleothermometer in the water column and sediments of the Santa Barbara Basin, California. Paleoceanography 22, 1–9.
Hurley, S.J., Lipp, J.S., Close, H.G., Hinrichs, K.-U., Pearson, A., 2018. Distribution and export of isoprenoid tetraether lipids in suspended particulate matter from the water column of the Western Atlantic Ocean. Organic Geochemistry 116, 90–102.

Iverson, V., Morris, R.M., Frazar, C.D., Berthiaume, C.T., Morales, R.L., Armbrust, E.V., 2012. Untangling genomes from metagenomes: revealing an uncultured class of marine Euryarchaeota. Science 335, 587–590.
Kalanetra, K.M., Bano, N., Hollibaugh, J.T., 2009. Ammonia-oxidizing archaea in the Arctic Ocean and Antarctic coastal waters. Environmental Microbiology 11, 2434–2445.
Karner, M.B., DeLong, E.F., Karl, D.M., 2001. Archaeal dominance in the mesopelagiczone of the Pacific Ocean. Nature 409, 507–510.
Kim, J.-H., Schouten, S., Hopmans, E.C., Donner, B., Sinninghe Damsté, J.S., 2008. Global sediment core-top calibration of the TEX_{86} paleothermometer in the ocean. Geochimica et Cosmochimica Acta 72, 1154–1173.
Kim, J.-H., Schouten, S., Rodrigo-Gámiz, M., Rampen, S., Marino, G., Huguet, C., Helmke, P., Buscail, R., Hopmans, E.C., Pross, J., Sangiorgi, F., Middelburg, J.B.M., Sinninghe Damsté, J.S., 2015. Influence of deep-water derived isoprenoid tetraether lipids on the TEX_{86}^{H} paleothermometer in the Mediterranean Sea. Geochimica et Cosmochimica Acta 150, 125–141.
Kim, J.-H., van der Meer, J., Schouten, S., Helmke, P., Willmott, V., Sangiorgi, F., Koç, N., Hopmans, E.C., Sinninghe Damsté, J.S., 2010. New indices and calibrations derived from the distribution of crenarchaeal isoprenoid tetraether lipids, Implications for past sea surface temperature reconstructions. Geochimica et Cosmochimica Acta 74, 4639–4654.
Kim, J.-H., Villanueva, L., Zell, C., Sinninghe Damsté, J.S., 2016. Biological source and provenance of deep-water derived isoprenoid tetraether lipids along the Portuguese continental margin. Geochimica et Cosmochimica Acta 172, 177–204.
Kim, J., Crosta, X., Willmott, V., Renssen, H., Bonnin, J., Helmke, P., Schouten, S., Sinninghe Damsté, J.S., 2012. Holocene subsurface temperature variability in the eastern Antarctic continental margin. Geophysical Research Letters 39, 1–6.
Klindworth, A., Pruesse, E., Schweer, T., Peplies, J., Quast, C., Horn, M., Glockner, F.O., 2013. Evaluation of general 16S ribosomal RNA gene PCR primers for classical and next-generation sequencing-based diversity studies. Nucleic Acids Research 41, 1–11.
Krom, M.D., Kress, N., Brenner, S., Gordon, L.I., 1991. Phosphorus limitation of primary productivity in the eastern Mediterranean Sea. Limnology and Oceanography 36, 424–432.
Kumar, S., Stecher, G., Tamura, K., 2016. MEGA7: Molecular evolutionary genetics analysis version 7.0 for bigger datasets. Molecular Biology and Evolution 33, 1870–1874.
La Cono, V., Ruggeri, G., Azzaro, M., Crisafi, F., Decembrini, F., Denaro, R., La Spada, G., Maimone, G., Monticelli, L.S., Smedile, F., Giuliano, L., Yakimov, M.M., 2018. Contribution of bicarbonate assimilation to carbon pool dynamics in the deep Mediterranean Sea and cultivation of actively nitrifying and CO_2-fixing bathypelagic prokaryotic consortia. Frontiers in Microbiology 9, 1–18.
Letunic, I., Bork, P., 2016. Interactive tree of life (iTOL) v3: an online tool for the display and annotation of phylogenetic and other trees. Nucleic Acids Research 44, W242–W245.
Lincoln, S.A., Wai, B., Eppley, J.M., Church, M.J., Summons, R.E., DeLong, E.F., 2014. Planktonic Euryarchaeota are a significant source of archaeal tetraether lipids in the ocean. Proceedings of the National Academy of Sciences of the United States of America 111, 9858–9863.
Lopes dos Santos, R.A., Prange, M., Castañeda, I.S., Schefuß, E., Mulitza, S., Schulz, M., Niedermeyer, E.M., Sinninghe Damsté, J.S., Schouten, S., 2010. Glacial–interglacial variability in Atlantic meridional overturning circulation and thermocline adjustments in the tropical North Atlantic. Earth and Planetary Science Letters 300, 407–414.
Ludwig, W., Strunk, O., Westram, R., Richter, L., Meier, H., Yadhukumar, Buchner, A., Lai, T., Steppi, S., Jobb, G., Förster, W., Brettske, I., Gerber, S., Ginhart, A.W., Gross, O., Grumann, S., Hermann, S., Jost, R., König, A., Liss, T., Lüssmann, R., May, M., Nonhoff, B., Reichel, B., Strehlow, R., Stamatakis, A., Stuckmann, N., Vilbig, A., Lenke, M., Ludwig, T., Bode, A., Schleifer, K.-H., 2004. ARB: a software environment for sequence data. Nucleic Acids Research 32, 1363–1371.
Martin-Cuadrado, A.-B., Garcia-Heredia, I., Moltó, A.G., López-Úbeda, R., Kimes, N., López-García, P., Moreira, D., Rodriguez-Valera, F., 2014. A new class of marine Euryarchaeota group II from the Mediterranean deep chlorophyll maximum. The ISME Journal 9, 1–16.
Massana, R., Delong, E.F., Pedrós-Alió, C., 2000. A few cosmopolitan phylotypes dominate planktonic archaeal assemblages in widely different oceanic provinces. Applied and Environmental Microbiology 66, 1777–1787.
MEDOC group, 1970. Observation of formation of deep water in the Mediterranean Sea, 1969. Nature 227, 1037–1040.
Menzel, D., Hopmans, E.C., Schouten, S., Sinninghe Damsté, J.S., 2006. Membrane tetraether lipids of planktonic Crenarchaeota in Pliocene sapropels of the eastern Mediterranean Sea. Palaeogeography, Palaeoclimatology, Palaeoecology 239, 1–15.
Mincer, T.J., Church, M.J., Taylor, L.T., Preston, C., Karl, D.M., DeLong, E.F., 2007. Quantitative distribution of presumptive archaeal and bacterial nitrifiers in Monterey Bay and the North Pacific Subtropical Gyre. Environmental Microbiology 9, 1162–1175.
Moore, E.K., Villanueva, L., Hopmans, E.C., Rijpstra, W.I.C., Mets, A., Dedysh, S.N., Sinninghe Damsté, J.S., 2015. Abundant trimethylornithine lipids and specific gene sequences are indicative of planctomycete importance at the oxic/anoxic interface in *Sphagnum*-dominated northern wetlands. Applied and Environmental Microbiology 81, 6333–6344.
Park, S.-J., Ghai, R., Martín-Cuadrado, A.-B., Rodríguez-Valera, F., Chung, W.-H., Kwon, K., Lee, J.-H., Madsen, E.L., Rhee, S.-K., 2014. Genomes of two new ammonia-oxidizing archaea enriched from deep marine sediments. PLoS ONE 9, 1–10.
Pitcher, A., Hopmans, E.C., Mosier, A.C., Park, S.-J., Rhee, S.-K., Francis, C.A., Schouten, S., Sinninghe Damsté, J.S., 2011a. Core and intact polar glycerol dibiphytanyl glycerol tetraether lipids of ammonia-oxidizing archaea enriched from marine and estuarine sediments. Applied and Environmental Microbiology 77, 3468–3477.
Pitcher, A., Villanueva, L., Hopmans, E.C., Schouten, S., Reichart, G.-J., Sinninghe Damsté, J.S., 2011b. Niche segregation of ammonia-oxidizing archaea and anammox bacteria in the Arabian Sea oxygen minimum zone. The ISME Journal 5, 1896–1904.
Polik, C.A., Elling, F.J., Pearson, A., 2018. Impacts of paleoecology on the TEX_{86} sea surface temperature proxy in the Pliocene-Pleistocene Mediterranean Sea. Paleoceanography and Paleoclimatology 33, 1–18.
Pollak, M.I., 1951. The sources of the deep water of the eastern Mediterranean Sea. Journal of Marine Research 10, 128–152.
Quast, C., Pruesse, E., Yilmaz, P., Gerken, J., Schweer, T., Yarza, P., Peplies, J., Glöckner, F.O., 2013. The SILVA ribosomal RNA gene database project: improved data processing and web-based tools. Nucleic Acids Research 41, D590–D596.
Rinke, C., Schwientek, P., Sczyrba, A., Ivanova, N.N., Anderson, I.J., Cheng, J.-F., Darling, A.E., Malfatti, S., Swan, B.K., Gies, E.A., Dodsworth, J.A., Hedlund, B.P., Tsiamis, G., Sievert, S.M., Liu, W.-T., Eisen, J.A., Hallam, S.J., Kyrpides, N.C., Stepanauskas, R., Rubin, E.M., Hugenholtz, P., Woyke, T., 2013. Insights into the phylogeny and coding potential of microbial dark matter. Nature 499, 431–437.
Roether, W., Manca, B.B., Klein, B., Bregant, D., Georgopoulos, D., Beitzel, V., Kovaeevic, V., Luchetta, A., 1996. Recent changes in Eastern Mediterranean deep waters. Science 271, 30–32.
Saitou, N., Nei, M., 1987. The neighbor-joining method: a new method for reconstructing phylogenetic trees. Molecular Biology and Evolution 4, 406–425.
Schouten, S., Hopmans, E.C., Baas, M., Boumann, H., Standfest, S., Könneke, M., Stahl, D.A., Sinninghe Damsté, J.S., 2008. Intact membrane lipids of "*Candidatus* Nitrosopumilus maritimus", a cultivated representative of the cosmopolitan mesophilic group I crenarchaeota. Applied and Environmental Microbiology 74, 2433–2440.
Schouten, S., Hopmans, E.C., Schefuβ, E., Sinninghe Damsté, J.S., 2002. Distributional variations in marine crenarchaeotal membrane lipids: a new tool for reconstructing ancient sea water temperatures? Earth and Planetary Science Letters 204, 265–274.
Schouten, S., Hopmans, E.C., Sinninghe Damsté, J.S., 2013. The organic geochemistry of glycerol dialkyl glycerol tetraether lipids: a review. Organic Geochemistry 54, 19–61.
Schouten, S., Pitcher, A., Hopmans, E.C., Villanueva, L., van Bleijswijk, J., Sinninghe Damsté, J.S., 2012. Intact polar and core glycerol dibiphytanyl glycerol tetraether lipids in the Arabian Sea oxygen minimum zone: I. Selective preservation and degradation in the water column and consequences for the TEX_{86}. Geochimica et Cosmochimica Acta 98, 228–243.
Schouten, S., Villanueva, L., Hopmans, E.C., van der Meer, M.T.J., Sinninghe Damsté, J. S., 2014. Are Marine Group II Euryarchaeota significant contributors to tetraether lipids in the ocean? Proceedings of the National Academy of Sciences of the United States of America 111, E4285.
Schubotz, F., Wakeham, S.G., Lipp, J.S., Fredricks, H.F., Hinrichs, K.-U., 2009. Detection of microbial biomass by intact polar membrane lipid analysis in the water column and surface sediments of the Black Sea. Environmental Microbiology 11, 2720–2734.
Sinninghe Damsté, J.S., Rijpstra, W.I.C., Hopmans, E.C., den Uijl, M.J., Weijers, J.W.H., Schouten, S., 2018. The enigmatic structure of the crenarchaeol isomer. Organic Geochemistry 124, 22–28.
Sinninghe Damsté, J.S., Rijpstra, W.I.C., Hopmans, E.C., Jung, M.-Y., Kim, J.-G., Rhee, S.-K., Stieglmeier, M., Schleper, C., 2012. Intact polar and core glycerol dibiphytanyl glycerol tetraether lipids of group I.1a and I.1b Thaumarchaeota in soil. Applied and Environmental Microbiology 78, 6866–6874.
Sinninghe Damsté, J.S., Rijpstra, W.I.C., Hopmans, E.C., Prahl, F.G., Wakeham, S.G., Schouten, S., 2002a. Distribution of membrane lipids of planktonic crenarchaeota in the Arabian Sea. Applied and Environmental Microbiology 68, 2997–3002.
Sinninghe Damsté, J.S., Schouten, S., Hopmans, E.C., van Duin, A.C.T., Geenevasen, J. A.J., 2002b. Crenarchaeol: the characteristic core glycerol dibiphytanyl glycerol tetraether membrane lipid of cosmopolitan pelagic crenarchaeota. Journal of Lipid Research 43, 1641–1651.
Sintes, E., Bergauer, K., De Corte, D., Yokokawa, T., Herndl, G.J., 2013. Archaeal *amo*A gene diversity points to distinct biogeography of ammonia-oxidizing *Crenarchaeota* in the ocean. Environmental Microbiology 15, 1647–1658.
Sintes, E., De Corte, D., Haberleitner, E., Herndl, G.J., 2016. Geographic distribution of archaeal ammonia oxidizing ecotypes in the Atlantic Ocean. Frontiers in Microbiology 7, 1–14.
Smith, J.M., Damashek, J., Chavez, F.P., Francis, C.A., 2016. Factors influencing nitrification rates and the abundance and transcriptional activity of ammonia-oxidizing microorganisms in the dark northeast Pacific Ocean. Limnology and Oceanography 61, 596–609.
Sollai, M., Villanueva, L., Hopmans, E.C., Reichart, G.-J., Sinninghe Damsté, J.S., 2018. A combined lipidomic and 16S rRNA gene amplicon sequencing approach reveals archaeal sources of intact polar lipids in the stratified Black Sea water column. Geobiology 17, 1–19.
Strickland, J.D.H., Parsons, T.R., 1968. A Practical Handbook of Seawater Analysis. Queen's Printer, Ottawa.

Sverdrup, H.U., Johnson, M.W., Flemming, R.H., 1942. The Oceans – Their Physics, Chemistry, and General Biology. Prentice-Hall, New York.
Sturt, H.F., Summons, R.E., Smith, K., Elvert, M., Hinrichs, K.-U., 2004. Intact polar membrane lipids in prokaryotes and sediments deciphered by high-performance liquid chromatography/electrospray ionization multistage mass spectrometry—new biomarkers for biogeochemistry and microbial ecology. Rapid Communications in Mass Spectrometry 18, 617–628.
Tamburini, C., Garel, M., Al Ali, B., Mérigot, B., Kriwy, P., Charrière, B., Budillon, G., 2009. Distribution and activity of Bacteria and Archaea in the different water masses of the Tyrrhenian Sea. Deep-Sea Research Part II: Topical Studies in Oceanography 56, 700–712.
Taylor, K.W.R., Huber, M., Hollis, C.J., Hernandez-Sanchez, M.T., Pancost, R.D., 2013. Re-evaluating modern and Paleogene GDGT distributions: Implications for SST reconstructions. Global and Planetary Change 108, 158–174.
Techtmann, S.M., Fortney, J.L., Ayers, K.A., Joyner, D.C., Linley, T.D., Pfiffner, S.M., Hazen, T.C., 2015. The unique chemistry of Eastern Mediterranean water masses selects for distinct microbial communities by depth. PLoS ONE 10, 1–22.
Teira, E., Lebaron, P., Van Aken, H., Herndl, G.J., 2006. Distribution and activity of Bacteria and Archaea in the deep water masses of the North Atlantic. Limnology and Oceanography 51, 2131–2144.
Thompson, J.D., Higgins, D.G., Gibson, T.J., 1994. CLUSTAL W: improving the sensitivity of progressive multiple sequence alignment through sequence weighting, position-specific gap penalties and weight matrix choice. Nucleic Acids Research 22, 4673–4680.
Tierney, J.E., Tingley, M.P., 2015. A TEX_{86} surface sediment database and extended Bayesian calibration. Scientific Data 2, 1–10.
Trommer, G., Siccha, M., van der Meer, M.T.J., Schouten, S., Sinninghe Damsté, J.S., Schulz, H., Hemleben, C., Kucera, M., 2009. Distribution of Crenarchaeota tetraether membrane lipids in surface sediments from the Red Sea. Organic Geochemistry 40, 724–731.
Turich, C., Freeman, K.H., Bruns, M.A., Conte, M., Jones, A.D., Wakeham, S.G., 2007. Lipids of marine Archaea: Patterns and provenance in the water-column and sediments. Geochimica et Cosmochimica Acta 71, 3272–3291.
Villanueva, L., Schouten, S., Sinninghe Damsté, J.S., 2017. Phylogenomic analysis of lipid biosynthetic genes of Archaea shed light on the "lipid divide". Environmental Microbiology 19, 54–69.
Winter, C., Kerros, M.-E., Weinbauer, M.G., 2009. Seasonal changes of bacterial and archaeal communities in the dark ocean: evidence from the Mediterranean Sea. Limnology and Oceanography 54, 160–170.
Wüst, G., 1961. On the vertical circulation of the Mediterranean Sea. Journal of Geophysical Research 66, 3261–3271.
Yakimov, M.M., Cono, V.La., Smedile, F., DeLuca, T.H., Juárez, S., Ciordia, S., Fernández, M., Albar, J.P., Ferrer, M., Golyshin, P.N., Giuliano, L., 2011. Contribution of crenarchaeal autotrophic ammonia oxidizers to the dark primary production in Tyrrhenian deep waters (Central Mediterranean Sea). The ISME Journal 5, 945–961.
Zavaterelli, M., Mellor, G.L., 1995. A numerical study of the Mediterranean Sea circulation. Journal of Physical Oceanography 25, 1384–1414.
Zhou, J., Song, X., Zhang, C.Y., Chen, G.F., Lao, Y.M., Jin, H., Cai, Z.H., 2018. Distribution patterns of microbial community structure along a 7000-mile latitudinal transect from the Mediterranean Sea across the Atlantic Ocean to the Brazilian coastal sea. Microbial Ecology 76, 1–18.
Zhu, C., Wakeham, S.G., Elling, F.J., Basse, A., Mollenhauer, G., Versteegh, G.J.M., Könneke, M., Hinrichs, K.-U., 2016. Stratification of archaeal membrane lipids in the ocean and implications for adaptation and chemotaxonomy of planktonic archaea. Environmental Microbiology 18, 4324–4336.